

## MicroRNA-155 Exerts Cell-Specific Antiangiogenic but Proarteriogenic Effects During Adaptive Neovascularization

Franziska Pankratz, MSc; Xavier Bemtgen, MD; Robert Zeiser, MD;

Franziska Leonhardt, PhD; Sheena Kreuzaler, BSc; Ingo Hilgendorf, MD, PhD;

Christian Smolka, PhD; Thomas Helbing, MD; Imo Hoefer, MD, PhD; Jennifer S. Esser, PhD;

Max Kustermann, MD; Martin Moser, MD; Christoph Bode, MD; Sebastian Grundmann, MD, PhD

**Background**—Adaptive neovascularization after arterial occlusion is an important compensatory mechanism in cardiovascular disease and includes both the remodeling of pre-existing vessels to collateral arteries (arteriogenesis) and angiogenic capillary growth. We now aimed to identify regulatory microRNAs involved in the modulation of neovascularization after femoral artery occlusion in mice.

**Methods and Results**—Using microRNA-transcriptome analysis, we identified miR-155 as a downregulated microRNA during hindlimb ischemia. Correspondingly, inhibition of miR-155 in endothelial cells had a stimulatory effect on proliferation and angiogenic tube formation via derepression of its direct target gene angiotensin II type 1 receptor. Surprisingly, miR-155-deficient mice showed an unexpected phenotype *in vivo*, with a strong reduction of blood flow recovery after femoral artery ligation (arteriogenesis) dependent on the attenuation of leukocyte-endothelial interaction and a reduction of proarteriogenic cytokine expression. Consistently, miR-155-deficient macrophages exhibit a specific alteration of the proarteriogenic cytokine expression profile, which is partly mediated by the direct miR-155 target gene SOCS-1.

**Conclusions**—Our data demonstrate that miR-155 exerts an antiangiogenic but proarteriogenic function in the regulation of neovascularization via the suppression of divergent cell-specific target genes and that its expression in both endothelial and bone marrow-derived cells is essential for arteriogenesis in response to hindlimb ischemia in mice. (*Circulation*. 2015;131:1575-1589. 10.1161/CIRCULATIONAHA.114.014579.)

**Key Words:** angiogenesis effect ■ microRNAs

During the course of atherosclerotic vascular disease, the adaptive growth of blood vessels is a naturally occurring process that can partly compensate for the decrease in blood flow after the narrowing or occlusion of a major artery. It includes both the sprouting of new endothelial capillaries (angiogenesis) and the enlargement of pre-existing arteriolar and arterial anastomoses to functional collateral arteries (arteriogenesis).<sup>1</sup> During angiogenesis, a drop in tissue oxygen tension results in increased expression of hypoxia-inducible transcription factors and cytokines, stimulating endothelial proliferation and sprouting in the ischemic tissue, improving distribution and use of the remaining blood flow. On the other hand, arteriogenesis is characterized by a well-orchestrated inflammatory response that is not restricted to the endothelial cell (EC) layer but facilitated by the perivascular infiltration of bone marrow-derived cell populations, mediating the proliferation of both endothelial and vascular smooth muscle cells. During the past decade, monocytes and macrophages were especially demonstrated to exert an important stimulatory function in the regulation

of collateral artery growth.<sup>2</sup> Although our knowledge about these contributing cell populations in the different forms of vascular growth steadily increases, our understanding of the basic regulatory principles controlling these processes is still limited. Other than canonical mediators of blood vessel growth, such as growth factors and their receptors, an additional functional group of regulators has recently emerged: microRNAs (miRNAs). These short (17–24 nucleotides), single-stranded regulatory RNA sequences are transcribed as precursor hairpin structures from intergenic or intronic regions of the genome that undergo several nuclear and cytoplasmatic processing steps to the mature miRNA.<sup>3</sup> Together with Argonaute proteins, they form the RNA-induced silencing complex and recognize specific sequences mostly located in the 3′ untranslated region of their target mRNA, resulting either in inhibition of translation or degradation of

Editorial see p 1533  
Clinical Perspective on p 1589

Received July 3, 2014; accepted March 3, 2015.

From Department of Cardiology and Angiology I, Heart Center, University of Freiburg, Germany (F.P., X.B., S.K., I.H., C.S., T.H., J.S.E., M.K., M.M., C.B., S.G.); Department of Biology, Albert-Ludwigs-University, Freiburg, Germany (F.P., F.L.); Department of Hematology and Oncology, University Hospital Freiburg, Germany (R.Z., F.L.); and Experimental Cardiology Laboratory, University Medical Center Utrecht, The Netherlands (I.H.).

The online-only Data Supplement is available with this article at <http://circ.ahajournals.org/lookup/suppl/doi:10.1161/CIRCULATIONAHA.114.014579/-DC1>.

Correspondence to Sebastian Grundmann, MD, PhD, Department of Cardiology and Angiology I, Heart Center, University of Freiburg, Hugstetter Str 55, 79106 Freiburg, Germany. E-mail [sebastian.grundmann@universitaets-herzzentrum.de](mailto:sebastian.grundmann@universitaets-herzzentrum.de)

© 2015 American Heart Association, Inc.

*Circulation* is available at <http://circ.ahajournals.org>

DOI: 10.1161/CIRCULATIONAHA.114.014579

the mRNA. Via tolerance of an imperfect complementarity, 1 miRNA can target several mRNA genes.

We now know that blood vessel growth is heavily modulated by miRNAs, because the genetic deletion of the miRNA-processing nuclease Dicer in mice results in early embryonic lethality attributed to vascular malformations.<sup>4</sup> Several individual miRNAs,<sup>5</sup> as well as polycistronic clusters,<sup>6</sup> have emerged as critical positive or as negative modulators of neovascularization. Our own group recently described the temporal expression profile of miRNAs after femoral artery occlusion in mice.<sup>7</sup> In the current study, we now extend this miRNA profiling approach to a further time point after induction of ischemia, revealing several additional candidate “angio-miRs,” including the multifunctional miR-155. We functionally characterize this miRNA in specific models of neovascularization in vitro and in vivo and identify miR-155 as a first miRNA with a divergent antiangiogenic but proarteriogenic function via the cell-intrinsic suppression of different target genes.

## Methods

A full Methods section is available in the online-only Data Supplement (Table I in the online-only Data Supplement).

### Hindlimb Ischemia

Animal protocols were approved by the Regierungspräsidium Freiburg (Germany), and all of the studies conformed to the Guide for the Care and Use of Laboratory Animals published by the directive 2010/63/EU of the European Parliament.

Unilateral femoral artery occlusion was performed in C57/BL6J and B6Cg-MiR-155<sup>tm1.1Rsky/J</sup> (miR-155<sup>-/-</sup>) mice under anesthesia with ketamine (100 mg/kg) and xylazine (2 mg/kg) by double ligation of the superficial femoral artery proximal and distal to the deep femoral artery. Animal numbers are stated with the different experimental results. A sham operation was performed on the contralateral leg.

### MiRNA Microarray Analysis

Analysis was performed as described previously.<sup>7</sup> In brief, total RNA from the distal adductor muscles at 6 time points after femoral artery ligation from 5 mice per time point was analyzed for all of the known murine miRNAs (miRBase 9.0) by a service provider (LC Sciences, Houston, TX). A complete raw data level of the microarray results was deposited at the National Center for Biotechnology Information gene expression and hybridization array data repository (Gene Expression Omnibus, <http://www.ncbi.nlm.nih.gov/geo/>) and can be accessed under the number GSE63212.

### Laser Doppler Perfusion Imaging

For laser Doppler perfusion imaging, the animals were anesthetized and measured under a Periscan PIM II imager (Perimed, Järfälla, Sweden). The readings of 3 individual measurements per mouse were averaged for each time point. Measurements were performed just before and after the operation on days 0, 14, and 28 with the last measurement constituting the main end point. Flow ratios of the occluded/nonoccluded leg were compared between the treatment groups.

### Statistical Analysis

Data are expressed as mean and SEM. Treatment groups were compared by unpaired Student *t* test with Prism 5 for Windows (GraphPad Software Inc, San Diego, CA).

One-way ANOVA was used for multiple comparisons of more than 2 groups. The Bonferroni posttest for multiple comparisons was used if the *P* value for the overall comparison was statistically significant (with the type of comparisons predetermined based on biological relevance). The unadjusted *P* value of each test was multiplied by the

number of comparisons. Differences were considered as significant if the resulting adjusted *P* value was <0.05.

Because normal distribution of our data could not be statistically verified for all of the experiments because of the sample size, additional nonparametric testing was performed with Mann-Whitney *U* tests (for 2 groups) for experiments shown in Figures 1A, 1C, 1D, 2F, 2H, 4G, 4L through 4R, 5D, 5I, 5J, 5L, 7H, and 7I. Values of *P*<0.05 were considered statistically significant.

## Results

### MiRNA Expression Profiling Reveals MiR-155 Downregulation During Hindlimb Ischemia

We explored the miRNA expression profile at 7 days after femoral artery ligation in mice, expanding our previously published miRNA-transcriptome profile<sup>7</sup> during neovascularization in this model for a second time point. After statistical testing and filtering for low gene expression, candidates for further analysis were selected based on the fold change of expression after induction of hindlimb ischemia compared with baseline levels.

Our hierarchical list of top regulated miRNAs (Tables 1 and 2) included previously described miRNA modulators of neovascularization, such as miRNA-100,<sup>7</sup> miRNA-106b,<sup>8</sup> miRNA-21,<sup>9</sup> and miRNA-214.<sup>10</sup> In addition, our experiment revealed a strong downregulation of miR-155, for which the role in adaptive blood vessel growth was so far unknown. Stem-loop-primer-based quantitative real-time polymerase chain reaction (PCR) analysis confirmed our microarray results and showed a significant decrease of miR-155 expression (Figure 1A). To visualize the cell type by which miR-155 was expressed we visualized LacZ under the control of the miR-155 promoter in vivo. MiR-155 was expressed in several tissue components, including striated muscle tissue and the vascular intima and media layers (Figure 1B). Because this technique allowed localization but not quantification of expression, we next used antibody-coupled magnetic beads to isolate CD31-positive ECs and F4/80-positive monocytes/macrophages at day 7 after femoral artery ligation and analyzed miR-155 expression by stem-loop-based TaqMan PCR. MiR-155 expression was significantly decreased in ECs, but no significant change in expression level could be observed in the F4/80-positive monocyte/macrophage population (Figure 1C and 1D).

### MiR-155 Is Downregulated by Angiogenic Cytokines and Exerts an Antiangiogenic Function in ECs via Suppression of AGTR1

In a next step we examined miR-155 expression in response to the proangiogenic stimuli vascular endothelial growth factor, as well as basic fibroblast growth factor (bFGF) and the proinflammatory mediator tumor necrosis factor (TNF)- $\alpha$  in human umbilical vein ECs. In good correspondence with the finding of miR-155 as a downregulated miRNA after hindlimb ischemia, we found a decrease in miR-155 expression after bFGF, as well as vascular endothelial growth factor stimulation (Figure 1E and 1F), whereas exposure to 8 hours of hypoxia did not result in significant upregulation or downregulation of miR-155 expression (Figure I in the online-only Data Supplement). Interestingly, miR-155 expression significantly increased under TNF- $\alpha$  stimulation (Figure 1G).

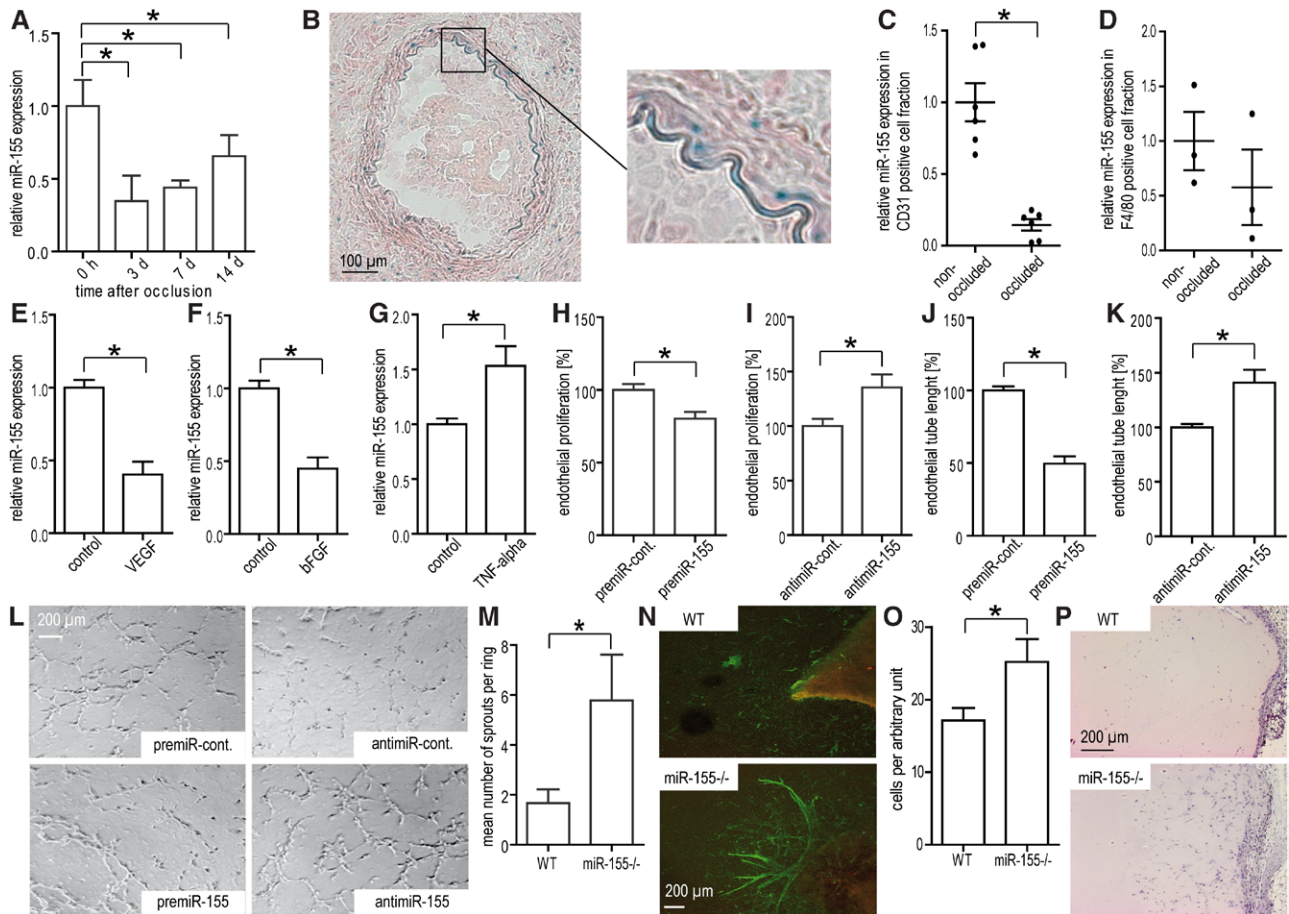


**Figure 1.** MicroRNA miR-155 expression is reduced after induction of hindlimb ischemia, and miR-155 modulates angiogenic properties of endothelial cells. **A**, MiR-155 expression after femoral artery occlusion at different time points as quantified by stem-loop-quantitative polymerase chain reaction (PCR; 5 animals per time point). **B**, MiR-155 expression visualized in ischemic hindlimb tissue of the miR-155-deficient mice by detecting *LacZ* expression under control of the miR-155 promoter. **C** and **D**, Quantification of miR-155 expression in different cell populations isolated by antibody-conjugated magnetic beads at day 7 after femoral artery ligation revealed a significant downregulation of miR-155 in CD31<sup>+</sup> endothelial cells (ECs;  $n=6$ ). **E** through **G**, Human umbilical vein ECs (HUVECs) were either stimulated with vascular endothelial growth factor (VEGF) or basic fibroblast growth factor (bFGF), which resulted in the decrease of miR-155 expression, or with tumor necrosis factor (TNF)- $\alpha$ , which increased miR-155 expression levels ( $n=6$ ). **H** and **I**, MiR-155 expression levels were modulated in HUVECs and proliferation was measured by MTT assay. Overexpression of miR-155 decreased proliferation, whereas an inhibition of this miRNA had the opposite effect ( $n=6$ ). **J** through **L**, Transfected HUVECs were cultured on Matrigel, and cumulative sprout length of capillary-like structures was measured. MiR-155 overexpression attenuated angiogenic tube formation, whereas miR-155 inhibition had a stimulatory effect ( $n=6$ ). **M**, Aortic rings lacking miR-155 showed more bFGF-induced microvessel sprouts compared with wild-type controls ( $n=9$ ). **N**, Representative pictures of aortic rings. Endothelial sprouts appeared in green, and red staining indicated vascular smooth muscle cells. **O** and **P**, Matrigel plug assay revealed a significantly increased number of infiltrating cells in plugs of miR-155-deficient mice compared with wild-type controls ( $n=10$ ). Data represent mean values with SEM. \* $P<0.05$  vs the corresponding control.

Based on these findings and after previous reports of miR-155 as an endothelial-enriched miRNA,<sup>11</sup> we analyzed miR-155 effects on angiogenic properties of cultured human umbilical vein ECs. MiR-155 was either overexpressed or inhibited by transfection with specific miR-155 precursor oligonucleotides (pre-miRs) or antisense-inhibitors (anti-miRs). Using a transfection protocol for miRNA modulation, we achieved a transfection efficacy of >90% and a significant positive or negative modulation of miRNA levels, respectively (Figure II in the online-only Data Supplement). Overexpression of miR-155 in ECs resulted in a significant attenuation of cellular proliferation (Figure 1H) and angiogenic tube formation, with a decrease in total sprout length in the 2-dimensional matrigel assay (Figure 1J and 1L). MiR-155 inhibition had a stimulatory effect

on both endothelial proliferation (Figure 1I) and tube formation (Figure 1K and 1L). To further support these in vitro findings and to exclude culture artifacts caused by the transfection procedure, we additionally performed an aortic ring assay with freshly isolated aortic tissue from wild-type and miR-155-deficient mice and found that a miR-155 deficiency in aortic rings enhanced bFGF-induced microvessel sprouts compared with wild-type ones (Figure 1M and 1N). We additionally performed an in vivo matrigel plug assay in wild-type and miR-155-deficient mice and found a significantly higher number of invading capillary vessels in matrigel of miR-155-deficient mice compared with wild-type controls (Figure 1O and 1P), which supports the notion of an overall inhibitory function of miR-155 on angiogenic properties of ECs.



**Table 1. Top 15 MicroRNAs Downregulated at Day 7 After Femoral Artery Occlusion as Identified by MicroRNA Microarray Analysis**

MicroRNA	Fold Change 7 d/Baseline
mmu-miR-101a	0.38
mmu-miR-101b	0.46
mmu-miR-328	0.48
mmu-miR-155	0.49
mmu-miR-378	0.60
mmu-miR-30e	0.60
mmu-miR-671	0.60
mmu-miR-133a*	0.65
mmu-miR-106b	0.67
mmu-miR-320	0.67
mmu-miR-29c	0.69
mmu-miR-451	0.69
mmu-miR-350	0.71
mmu-miR-100	0.72
mmu-miR-329	0.72

RNA of 5 mice per time point was pooled in equal amounts.

To reveal the miR-155 target gene responsible for these effects, we measured baseline mRNA expression levels of 84 validated or predicted miR-155 target genes in isolated wild-type and miR-155-deficient ECs using a PCR array and found *PU.1* and *AGTR1* to be the most enriched genes in ECs lacking miR-155 (Table II in the online-only Data Supplement). *AGTR1* is a well-known positive mediator of endothelial proliferation and sprouting,<sup>12</sup> and we found that *AGTR1* expression levels were modulated by overexpression or inhibition of miR-155 in human and murine ECs (Figure 2A and 2B). Simultaneous knockdown of *AGTR1* by small interfering RNA transfection (Figure III in the online-only Data Supplement) antagonized the stimulatory effects of miR-155 inhibitor treatment on EC proliferation (Figure 2E) and tube formation (Figure 2C and 2D). In addition, the number of sprouts was strongly reduced

**Table 2. Top 15 Upregulated MicroRNAs**

MicroRNA	Fold Change 7 d/Baseline
mmu-miR-346	12.14
mmu-miR-126-5p	5.71
mmu-miR-762	2.31
mmu-miR-223	1.91
mmu-miR-98	1.89
mmu-miR-342	1.84
mmu-miR-21	1.79
mmu-miR-335	1.65
mmu-miR-382	1.59
mmu-miR-30e*	1.57
mmu-miR-214	1.57
mmu-miR-705	1.54
mmu-miR-15b	1.53
mmu-miR-196a	1.50

in miR-155-deficient aortic rings if *AGTR1* was silenced (Figure 2F and 2G), demonstrating that *AGTR1* expression was necessary for the mediation of the antiangiogenic miR-155 effects in ECs. In vivo, we could detect a significantly increased *AGTR1* expression level in peroneus muscle tissue after femoral artery ligation, corresponding with the downregulation of miR-155 (Figure 2H).

### MiR-155 Deficiency Attenuates Perfusion Restoration and Leukocyte Infiltration

Our next aim was to investigate the effects of genetic miR-155 deficiency in vivo. We subjected miR-155-deficient mice and wild-type controls to unilateral femoral artery ligation and determined blood flow recovery. Surprisingly, flow restoration on day 14 (Figure 3A and 3B) and day 28 (Figure 3C and 3D) was significantly attenuated in miR-155-deficient mice in contrast to our in vitro findings, where miR-155 inhibition resulted in a stimulation of angiogenesis. Furthermore, we could detect a significant reduction of infiltrating CD11b-positive leukocytes in hindlimb tissue in miR-155-deficient mice (Figure 3E and 3F). Because this cell population is well documented to be a critical mediator of adaptive arteriogenesis, we hypothesized that a defect in monocyte infiltration could be responsible for the observed functional deficiency in blood flow restoration. The proarteriogenic function of this cell population is partly mediated by the expression of stimulatory cytokines and growth factors, and we detected a significant reduction in TNF- $\alpha$  mRNA levels in miR-155-deficient mice (Figure 3G). We therefore went on to characterize the arteriogenic phenotype of miR-155-deficient monocytes/macrophages and examined leukocyte-endothelial interaction and migration of circulating cells in this mouse strain.

### MiR-155 Deficiency Reduces Leukocyte-Endothelial Interaction and Migration of Macrophages

Intravital imaging of mesenteric venules after systemic TNF- $\alpha$  treatment showed a lower number of interacting leukocytes on the endothelial surface in miR-155-deficient mice (Figure 4A and 4B). To assess whether the migration of monocytes/macrophages as the subsequent step of proarteriogenic cell infiltration was also effected, we cultured bone marrow cells (BMCs) from miR-155-deficient and wild-type mice differentiated to the monocyte/macrophage lineage by macrophage colony-stimulating factor 1 stimulation (Figure IV in the online-only Data Supplement). In a transwell assay, bone marrow-derived macrophages (BMDMs) deficient for miR-155 showed an, on average, 80% reduction in migration capacity compared with wild-type cells (Figure 4C).

Because the migration of monocytes in vivo can differ from the in vitro observation, we subsequently investigated leukocyte infiltration in vivo in a model of sterile-induced peritonitis. Leukocyte migration into the peritoneal cavity was significantly reduced in miR-155-deficient animals (Figure 4D), whereas baseline blood leukocyte count did not differ between the mouse strains (Figure V in the online-only Data Supplement).

### Proarteriogenic Cytokine/Chemokine Production Is Impaired in miR-155-Deficient Macrophages

Following the observations that miR-155 influenced the leukocyte-endothelial interaction but also mediated angiogenic

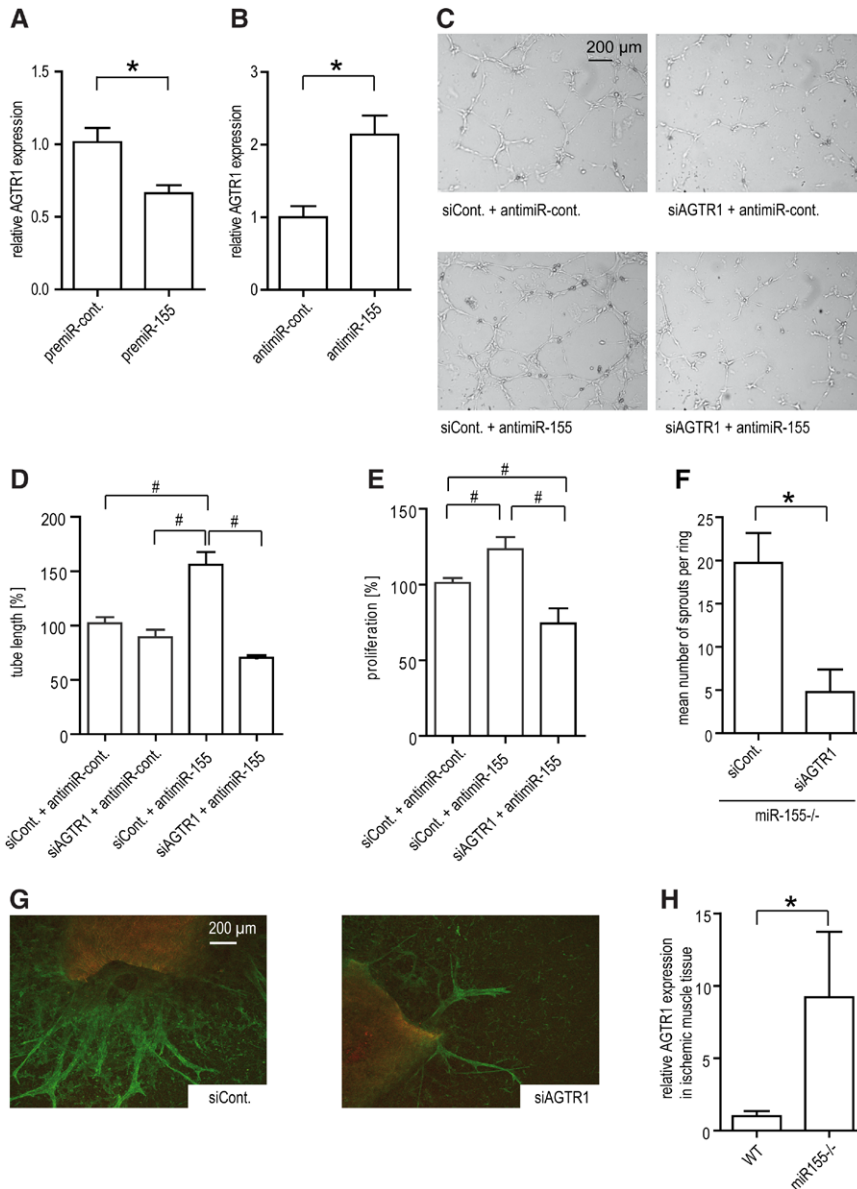


**Figure 2.** Antiangiogenic properties of microRNA miR-155 in human endothelial cells are mediated by its direct target, AGTR1. **A** and **B**, MiR-155 regulated angiotensin II receptor type I (AGTR1) expression. MiR-155 expression levels were modulated in human umbilical vein endothelial cells (HUVECs), and AGTR1 expression levels were determined by real-time polymerase chain reaction (PCR;  $n=7$ ). **C** through **E**, Concomitant silencing of miR-155 and AGTR1 led to a reduction of cumulative sprout length in 2-dimensional Matrigel assay ( $n \geq 6$ ) and proliferation in the MTT metabolization assay compared with single miR-155 inhibition ( $n=6$ ). **F** and **G**, Aortic rings lacking miR-155<sup>-/-</sup> showed less basic fibroblast growth factor (bFGF)-induced sprouts if AGTR1 was silenced ( $n=9$ ). Endothelial sprouts appeared in green, and red indicated vascular smooth muscle cells. **H**, AGTR1 expression level in peroneus muscle tissue was increased in miR-155<sup>-/-</sup> mice at day 7 after femoral artery ligation ( $n=6$ ). Data represent mean values with SEM. \* $P < 0.05$  vs the corresponding control. #Bonferroni corrected level of significance  $< 0.05$  vs the corresponding group.

sprouting and proliferation in ECs, we screened for baseline miR-155 expression level in different human and murine vascular and circulating cell populations and found a strongly enriched miR-155 expression in circulating cells (Figure 4E and 4F). Next, we examined the regulation of miR-155 in BMDMs in response to different proarteriogenic and proangiogenic stimuli. Although stimulation with TNF- $\alpha$  and monocyte chemoattractant protein (MCP) 1 increased miR-155 expression (Figure 4G and 4H), stimulation with TGF- $\beta$  and bFGF decreased miR-155 expression (Figure 4I and 4J), indicating a divergent regulation of miR-155 in the different forms of vascular growth. Hypoxia seemed not to be the main stimulus for miR-155 expression, because exposure to 8 hours of hypoxia did not significantly affect miR-155 expression (Figure 4K). After infiltration into the perivascular space, macrophages especially stimulate neovascularization by the secretion of proarteriogenic cytokines and growth factors. We and others recently described an essential role of the proinflammatory cytokine TNF- $\alpha$  in the stimulation of collateral artery growth

via activation of the p55 receptor.<sup>13,14</sup> We now found that miR-155-deficient BMDMs showed no significant difference in TNF- $\alpha$  expression at baseline. However, after lipopolysaccharide stimulation, miR-155<sup>-/-</sup> macrophages exhibited a significantly impaired TNF- $\alpha$  secretion (Figure 4L). Because these findings suggested a possible alteration of the arteriogenic cytokine expression profile, we compared the expression of 84 key inflammatory cytokines and receptors in miR-155-deficient macrophages with wild-type cells after lipopolysaccharide stimulation using a quantitative real-time PCR array. Among the top 10 downregulated molecules in miR-155-deficient macrophages were the chemoattractant proteins MCP-1 and MCP-5, as well as the proinflammatory mediator macrophage inflammatory protein (MIP)-1 $\beta$  (Table III in the online-only Data Supplement), and we could also confirm a significantly reduced expression on protein level (Figure 4O through 4Q), suggesting a defect in proarteriogenic cytokine production under conditions of miR-155 deficiency. In addition, we characterized apoptosis level in wild-type and miR-155-deficient

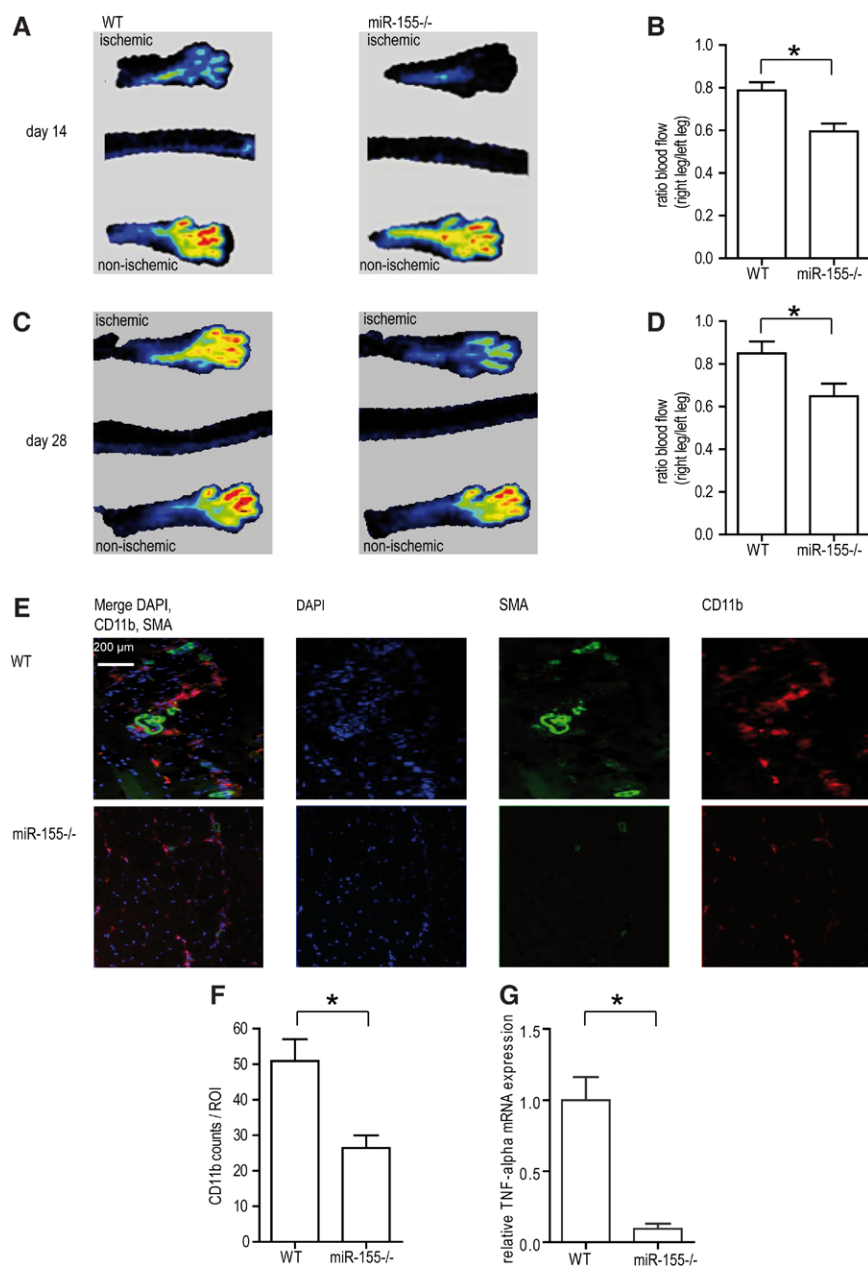


**Figure 3.** MicroRNA miR-155 deficiency results in attenuated perfusion restoration after femoral artery occlusion in vivo. **A** through **D**, Laser Doppler measurement revealed a reduction in blood flow recovery of miR-155<sup>-/-</sup> mice compared with controls at days 14 and 28 after induction of ischemia (n=10). **E** and **F**, MiR-155<sup>-/-</sup> mice showed a decrease in infiltrating CD11b<sup>+</sup> leukocytes, shown in the overlay by a red CD11b staining. Blood vessels appear in green and nuclei in blue (n=10). **G**, Real-time polymerase chain reaction (PCR)-based analysis showed that tumor necrosis factor (TNF)- $\alpha$  expression at the area of neovascularization was reduced in miR-155<sup>-/-</sup> mice (n=10). Data represent mean values with SEM. \*P<0.05 vs the corresponding control.

macrophages using a luminogenic assay and found increased caspase-3 and -7 activities in macrophages lacking miR-155 (Figure 4R), which might also contributed to the lower number of perivascular leukocytes in the ischemic hindlimb tissue.

Because we found miR-155 to exert modulating function in BMDMs in vitro we went on with a phenotypic characterization of monocytes 14 days after femoral artery ligation in mice. The absolute number of circulating monocytes did not differ at baseline between miR-155-deficient mice and wild-type controls (Figure VIA in the online-only Data Supplement). However, a significantly lower increase in the absolute number of circulating monocytes after induction of hindlimb ischemia could be observed in mice lacking miR-155 (Figure VIE in the online-only Data Supplement). Additionally, the proinflammatory monocyte Ly6C<sup>hi</sup> subset was decreased in these mice (Figure VIF in the online-only Data Supplement). Corresponding with our in vitro data we

could show an impaired cytokine/chemokine production profile in Ly6C<sup>hi</sup> monocytes in vivo as, for example, MCP-1, TNF- $\alpha$ , and interleukin 6 were significantly reduced in miR-155-deficient mice compared with wild-type animals (Figure VII through VIP in the online-only Data Supplement).

### Direct MiR-155 Target SOCS-1 Is Highly Expressed During Neovascularization in MiR-155-Deficient Mice and Confers Its Effect on the Arteriogenic Phenotype of Macrophages

To identify the direct miR-155 target in monocytes/macrophages responsible for the observed phenotypic differences in miR-155-deficient cells, we screened for cell-specific enrichment of 84 predicted or validated miR-155 target genes by PCR array analysis in BMDMs lacking miR-155 in comparison with wild-type cells (Table IVA and IVB in the online-only Data Supplement). This analysis identified

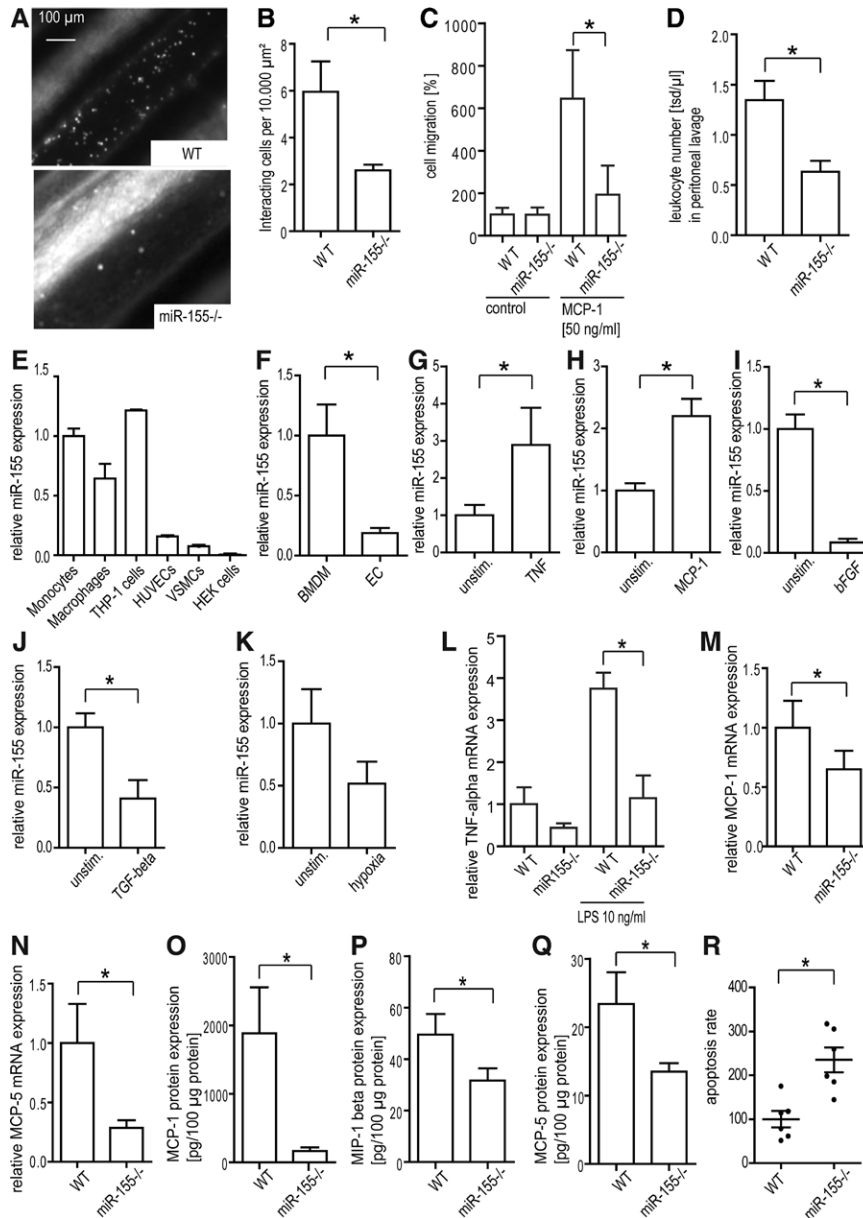


**Figure 4.** MicroRNA miR-155 deficiency attenuates leukocyte-endothelial interaction, as well as migration of leukocytes, and the proarteriogenic cytokine/chemokine production in miR-155<sup>-/-</sup> macrophages. **A** and **B**, Intravital imaging of mesenteric venules after systemic tumor necrosis factor (TNF)- $\alpha$  treatment revealed a lower number of interacting leukocytes on the endothelial surface in miR-155<sup>-/-</sup> mice ( $n=7$ ). **C**, Migration capacity in response to monocyte chemoattractant protein (MCP)-1 (50 ng/mL) was reduced in miR155<sup>-/-</sup> bone marrow-derived macrophages (BMDMs) compared with wild-type cells, as determined by Transwell migration assay. **D**, Migration of monocytes/macrophages was impaired in miR-155<sup>-/-</sup> mice in vivo. Sterile peritonitis was induced, peritoneal exudates were collected 2 days later, and leukocyte number was determined ( $n\geq 11$ ). **E** and **F**, Relative miR-155 expression level in different circulating and vascular cell populations as determined by stem-loop-based TaqMan polymerase chain reaction (PCR;  $n\geq 6$ ). **G** through **J**, MiR-155 was upregulated 24 hours after TNF- $\alpha$  (10 ng/mL) and MCP-1 (10 ng/mL) stimulation of BMDMs, whereas a stimulation with basic fibroblast growth factor (bFGF; 25 ng/mL) and TGF- $\beta$  (10 ng/mL) decreased miR-155 expression level ( $n=6$ ). **K**, In contrast to the cytokine stimulations, exposure to 8 hours of hypoxia did not result in a statistically significant regulation of miR-155 in our experimental series ( $n=6$ ). **L**, Real-time polymerase chain reaction (PCR)-based quantification of TNF- $\alpha$  mRNA levels in BMDMs after lipopolysaccharide (LPS) stimulation (24 hours; 10 ng/mL) showed a reduced TNF- $\alpha$  expression in miR-155<sup>-/-</sup> macrophages ( $n\geq 10$ ). **M** and **N**, BMDMs lacking miR-155 showed a reduced expression of MCP-1 and MCP-5 on mRNA level ( $n=6$ ). **O** through **Q**, MCP-1, macrophage inflammatory protein (MIP)-1 $\beta$ , and MCP-5 protein expression level were decreased in miR-155<sup>-/-</sup> BMDMs, as determined by ELISA ( $n\geq 10$ ). **R**, Apoptosis was significantly increased if miR-155 was lacking in BMDMs. Apoptosis level in cells was examined by measuring caspase-3 and -7 activities ( $n=6$ ). Data represent mean values with SEM. \* $P<0.05$  vs the corresponding control.

the previously validated miR-155 target SOCS-1, a negative regulator of Janus kinase/signal transducers and activators of transcription signaling, as the most upregulated gene with a 70-fold enrichment in miR-155-deficient BMDMs. SOCS-1

was enriched in monocytic cells compared with vascular ones in mice and humans (Figure 5A and 5B), as well as in the ischemic hindlimb tissue of miR-155-deficient mice in comparison with wild-type controls (Figure 5C). Accordingly,



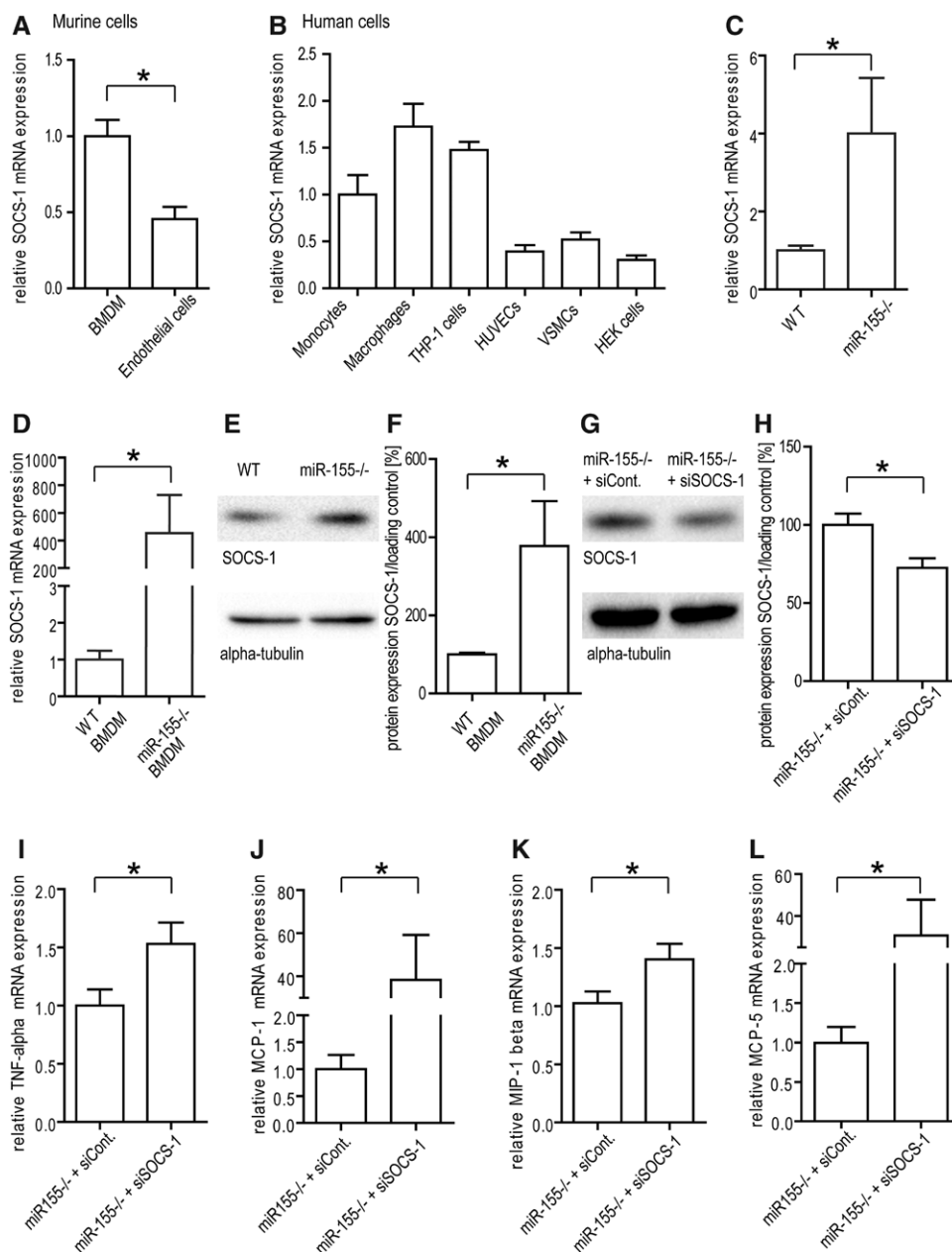


**Figure 5.** The direct microRNA miR-155 target SOCS-1 is highly expressed in circulating cells and confers its effects on the arteriogenic phenotype of macrophages. **A** and **B**, SOCS-1 was enriched in monocytes/macrophages compared with vascular cell lines in murine (**A**;  $n \geq 6$ ) and human cells (**B**), as shown by real-time polymerase chain reaction (PCR) analysis ( $n \geq 6$ ). **C**, SOCS-1 mRNA expression in the area of neovascularization isolated at day 7 after hindlimb ischemia was increased in miR-155<sup>-/-</sup> mice ( $n \geq 6$ ). **D** through **F**, SOCS-1 was enriched in miR155<sup>-/-</sup> bone marrow–derived macrophages (BMDMs) on mRNA expression level ( $n \geq 10$ ), as well as on protein level ( $n = 8$ ). **G** and **H**, SOCS-1 expression decreased in miR-155<sup>-/-</sup> BMDMs if SOCS-1 was silenced by specific small interfering RNA (siRNA;  $n = 6$ ). **I** through **L**, Silencing of SOCS-1 increased mRNA expression level of tumor necrosis factor (TNF)- $\alpha$ , monocyte chemoattractant protein (MCP)-1, macrophage inflammatory protein (MIP)-1 $\beta$ , and MCP-5 ( $n \geq 10$ ). BMDMs were either transfected with siRNA against SOCS-1 (siSOCS-1) or the respective control compound (siCont.), and mRNA expression levels were analyzed by real-time PCR. Data represent mean values with SEM. \* $P < 0.05$  vs the corresponding control.

BMDMs lacking miR-155 showed a significant derepression of SOCS-1 under basal culture conditions (Figure 5D through 5F). We went on to investigate whether silencing of the SOCS-1 expression level could rescue the phenotype of miR-155–deficient BMDMs (Figure 5G and 5H) and, indeed, silencing of SOCS-1 by small-interfering RNA (Figure VII in the online-only Data Supplement) led to an increase of TNF- $\alpha$ , MCP-1, MIP-1 $\beta$ , and MCP-5 expression in BMDMs lacking

miR-155, demonstrating that suppression of SOCS-1 is a necessary condition for the mediation of these proarteriogenic miR-155 effects (Figure 5I through 5L).

### MiR-155 Deficiency in Circulating Cells Is Sufficient for the Attenuation of Blood Flow Recovery

To assess whether the observed impairment in perfusion restoration after femoral artery ligation in miR-155–deficient



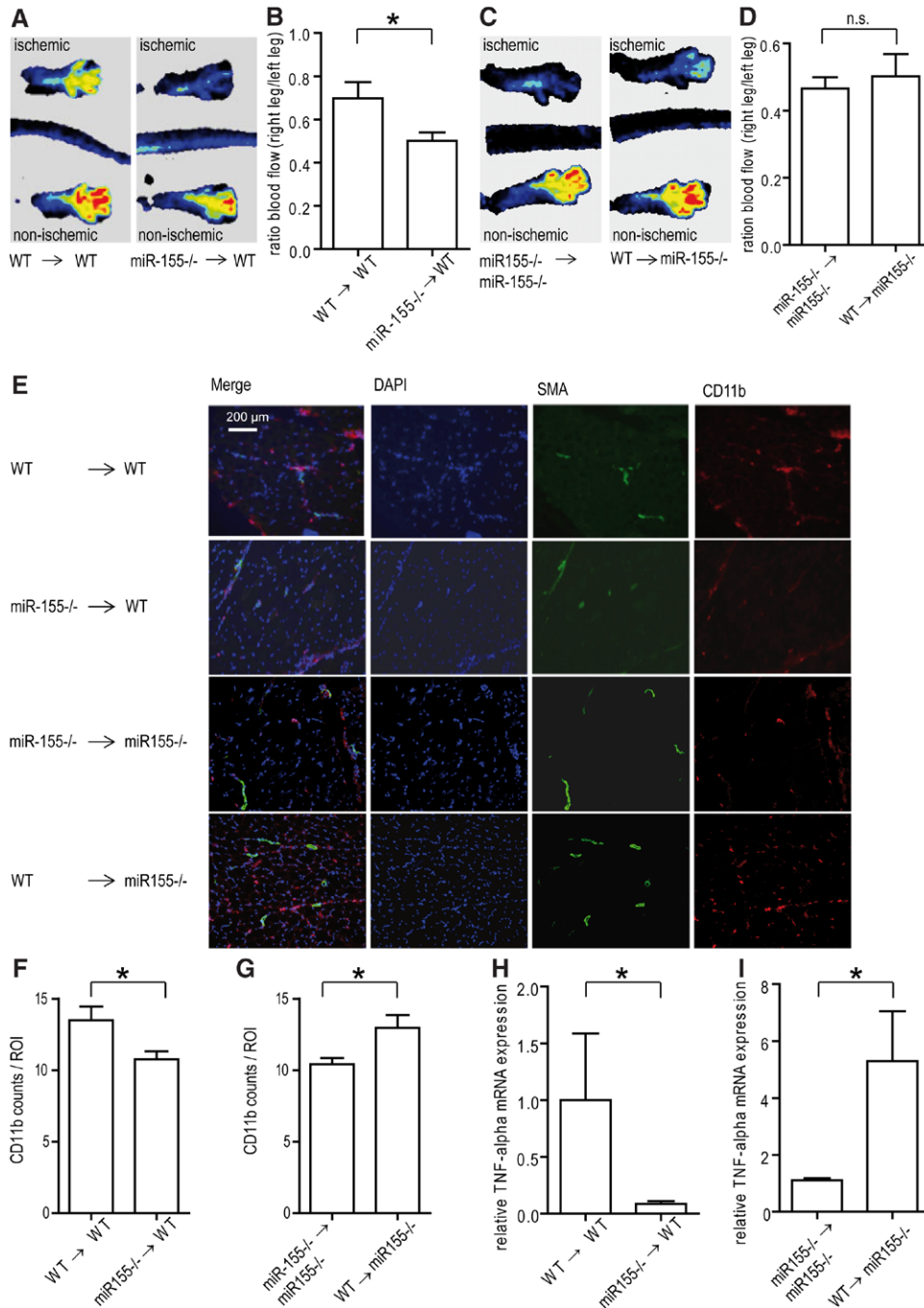


**Figure 6.** MicroRNA miR-155 deficiency in the hematopoietic system is sufficient for attenuation of blood flow recovery. Chimeric mice were generated by bone marrow transplantation, and hindlimb ischemia was induced 8 weeks later. **A** and **B**, Laser Doppler measurement at day 14 revealed a reduction in blood flow recovery of wild-type mice harboring miR-155<sup>-/-</sup> bone marrow cells (BMCs) compared with ones transplanted with miR-155<sup>+/+</sup> BMCs (n=12). **C** and **D**, Laser Doppler measurements were not significantly different between miR-155<sup>-/-</sup> recipients harboring miR-155<sup>-/-</sup> or miR-155<sup>+/+</sup> BMCs (n=10). **E** through **G**, MiR-155<sup>-/-</sup> deficiency in the hematopoietic system of miR-155<sup>+/+</sup> recipients led to decreased number of CD11b<sup>+</sup> leukocytes stained in red, whereas miR-155<sup>+/+</sup> BMCs in miR-155<sup>-/-</sup> mice enhanced the number of CD11b<sup>+</sup> cells (n=7). Arterial blood vessels were stained green and nuclei in blue. **H**, Real-time polymerase chain reaction (PCR)-based analysis of ischemic muscle tissue showed a reduction of tumor necrosis factor (TNF)-α expression in mice harboring miR-155<sup>-/-</sup> BMCs (n=8). **I**, TNF-α expression level increased if miR-155<sup>-/-</sup> recipients were transplanted with miR-155<sup>+/+</sup> BMCs (n≥6). Data represent mean values with SEM. \*P<0.05 vs the corresponding control.

mice can indeed be attributed to an miR-155 function in circulating cells, we performed bone marrow transplantation experiments (Figure VIII in the online-only Data Supplement). In good correspondence with our in vitro findings, miR-155 deficiency in bone marrow-derived cells

resulted in an impairment in perfusion restoration (Figure 6A and 6B). Also, a decreased number of infiltrating perivascular cells (Figure 6E and 6F), as well as a lower expression of the proarteriogenic cytokine TNF-α (Figure 6H), was detected in mice harboring miR-155<sup>-/-</sup> BMCs, mimicking the

phenotype of the global knockout. However, we did not find a significant difference in blood flow restoration between miR-155<sup>-/-</sup> recipients transplanted with miR-155<sup>+/+</sup> or miR-155<sup>-/-</sup> BMCs (Figure 6C and 6D), indicating that miR-155<sup>+/+</sup> expression exclusively in the hematopoietic system was not able to rescue the phenotype of a global knockout after hindlimb ischemia. Although reconstitution of miR-155<sup>-/-</sup> mice with wild-type BMCs resulted in a relative increase in the number of infiltrating CD11b<sup>+</sup> cells compared with the global knockout, the overall number remained below the values of wild-type controls (Figure 6G). In addition, TNF- $\alpha$  expression increased under reconstitution of global knockout with miR-155<sup>+/+</sup> BMCs (Figure 6I). We therefore hypothesized that miR-155 also directly affected vascular proinflammatory properties, independent of circulating cells.

### MiR-155 Deficiency in ECs Attenuates Adhesion Molecule Expression via an Increased Expression of AGTR1

We modulated miR-155 expression in murine ECs, and flow cytometric analysis showed a significant increase of intracellular adhesion molecule 1, as well as vascular cell adhesion molecule 1, expression after miR-155 overexpression (Figure 7A and 7C) and an attenuation under miR-155 suppression (Figure 7B and 7D). Next, we visualized endothelial activation *in vivo* by staining of intracellular adhesion molecule 1 with an intravenously injected fluorochrome-labeled antibody 4 hours after TNF- $\alpha$  injection. Intravital imaging of mesenteric venules revealed a strongly attenuated endothelial activation in miR-155-deficient mice compared with wild-type controls (Figure 7E and 7F). Taken together our findings indicated a regulation of murine adhesion molecule expression by miR-155. Again, these effects were mediated by the direct miR-155 target AGTR1, because its knockdown mimicked the effects of miR-155 overexpression (Figure 7L and 7M), and concomitant knockdown of miR-155 and AGTR1 abrogated the effect of single miR-155 inhibition on intracellular adhesion molecule 1 and vascular cell adhesion molecule 1 protein expression (Figure 7N and 7O).

Although AGTR1 is a predicted and validated miR-155 target in humans but not in mice (tested with the online target prediction tools Targetscan<sup>15–17</sup> and MiRanda<sup>18–20</sup>), our results on AGTR1 regulation showed that this regulatory pathway is conserved over species. In addition, our results demonstrate a direct modulation of AGTR1 by miR-155 by interacting with the murine AGTR1 3' untranslated region, for the first time validating this endothelial regulator as a direct miR-155 target gene in mice (Figure 7J and 7K).

### Discussion

Here, we describe a comprehensive miRNA expression profile after induction of hindlimb ischemia in mice, revealing the multifunctional miR-155 as one of the strongest downregulated miRNAs over time. In addition, we identify an antiangiogenic but proarteriogenic function of miR-155 in the regulation of adaptive blood vessel growth by the direct suppression of 2 functionally different target genes, SOCS-1, a negative feedback loop regulator of Janus kinase/signal transducers and activators of transcription signaling in monocytes/

macrophages, and AGTR1, a positive modulator of angiogenesis with anti-inflammatory effects in ECs.

Although we recently reported the first study applying differential expression results from an *in vivo* study to identify new regulators of neovascularization,<sup>7</sup> we now expanded our miRNA transcriptome profile for a later time point because we screened for miRNAs differentially expressed at day 7 after femoral artery occlusion in mice. Other than our previously described candidates, miR-100<sup>7</sup> and miR-214,<sup>10</sup> other already well characterized modulators of blood vessel growth are among the top upregulated and downregulated genes, such as miR-106b,<sup>8</sup> miR-21,<sup>9</sup> miR-378,<sup>21</sup> miR-29c,<sup>22</sup> miR-30e,<sup>23</sup> and miR-98<sup>24</sup>, whereby the last 4 named miRNAs are mainly known to modulate tumor angiogenesis. The validity of our screening approach is supported by the fact that Greco et al<sup>25</sup> also identified miR-29c as a downregulated miRNA in a similar setting. In addition, we found other miRNAs of potential interest that, until now, have not been functionally characterized in blood vessel growth and therefore could represent promising candidates for future studies, for example, the downregulated miR-329, which has so far been regarded as a brain-specific miRNA.<sup>26</sup> From our screening experiment, we selected miR-155 for further analysis because of its strong downregulation at days 3 to 14 after femoral artery ligation, its recently described enrichment in ECs,<sup>11,27</sup> and its known role in inflammatory signaling,<sup>28,29</sup> suggesting a potential functional involvement in hypoxia-driven angiogenesis or inflammation-mediated arteriogenesis.

Although a visualization of miR-155 expression in the hindlimb tissue confirmed previous reports of a broad expression in a wide variety of cell types,<sup>30</sup> our analysis of isolated ECs confirms that the downregulation of miR-155 in this cell population at least contributes to the overall regulation observed in our screening experiment. In addition, we find that miR-155 expression in ECs is controlled by the proangiogenic cytokines vascular endothelial growth factor and bFGF, suggesting a potential mechanism for this downregulation.

MiR-155 is expressed on the *BIC* locus on chromosome 21, and in the cardiovascular field miR-155 was first described in 2007 as a translational repressor of AGTR1 expression,<sup>31</sup> and a recent study in brain microvascular ECs reported an attenuating effect of miR-155 on EC morphogenesis.<sup>32</sup> Our current results demonstrate now for the first time that this regulatory interaction is conserved between humans and mice. This was relatively unexpected, because both miR-155 and AGTR1 sequences differ between the 2 species and context-score calculations by bioinformatic algorithms yield results below the cutoff for prediction of an miR-155-binding site in the AGTR1 mRNA. Because AGTR1 is not only an important controller of blood pressure and volume in the vascular system but also a strong stimulator of endothelial proliferation and tube formation,<sup>12</sup> we hypothesized that miR-155 could exert antiangiogenic properties in ECs via suppression of AGTR1. Indeed, this hypothesis is confirmed by our *in vitro* studies, in good correspondence with our *in vivo* findings that miR-155 expression decreases after induction of blood vessel growth. Concomitant knockdown of AGTR1 antagonizes the stimulatory effects of miR-155 inhibition. Although the targeting of additional mediators on angiogenic endothelial properties

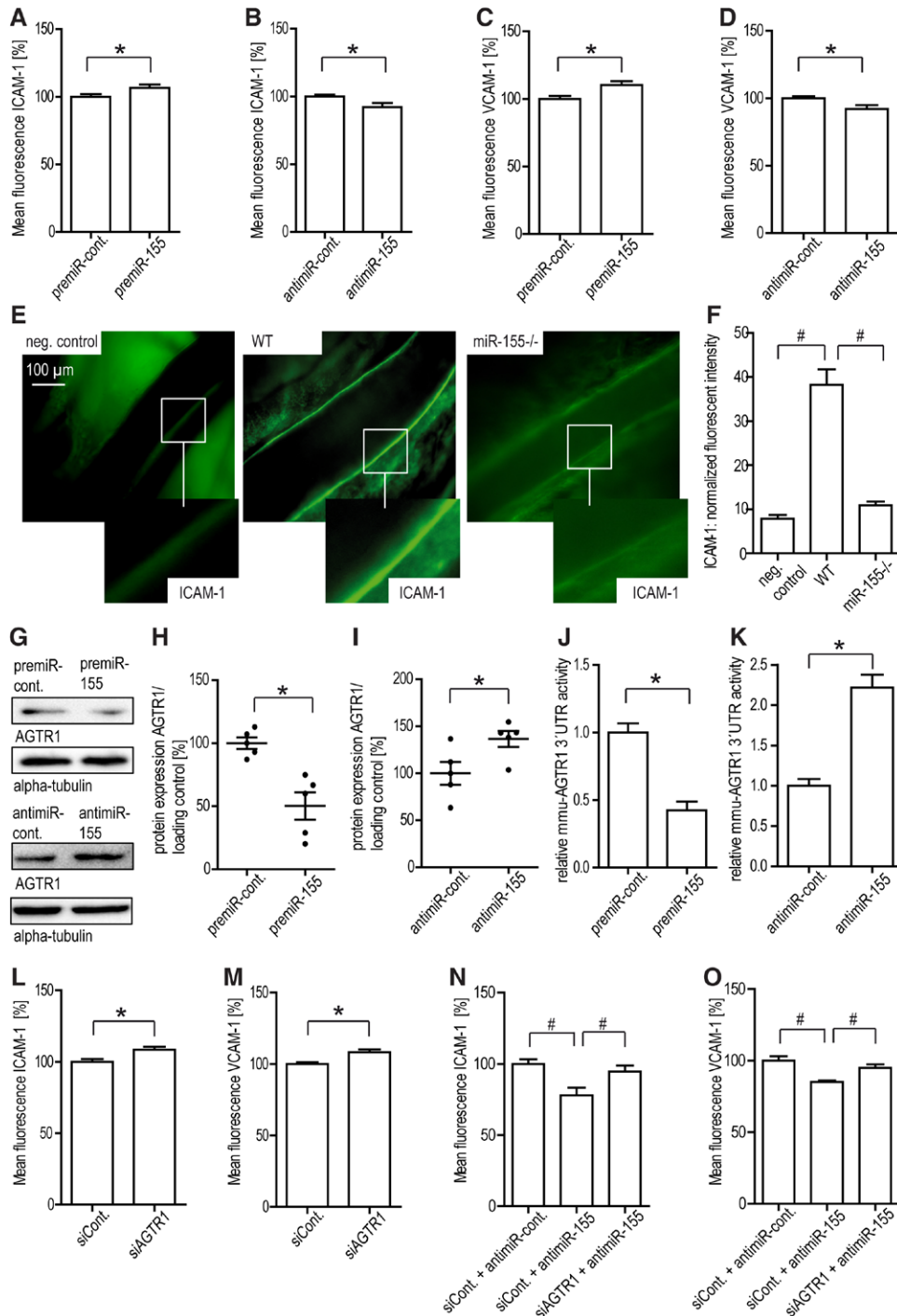


**Figure 7.** MicroRNA miR-155 regulates expression of adhesion molecules in murine endothelial cells by targeting AGTR1. **A** through **D**, Protein expression levels of intracellular adhesion molecule (ICAM) 1, as well as vascular cell adhesion molecule (VCAM) 1, were regulated by miR-155. MiR-155 expression levels were modulated in murine endothelial cells (ECs), and, after transfection, cells were stimulated with tumor necrosis factor (TNF)- $\alpha$  (10 ng/mL) for 12 hours, and surface protein expression levels of adhesion molecules were determined by flow cytometry (n=8). **E** and **F**, In vivo endothelial activation, displayed as ICAM-1 (in green) expression on endothelial surface, was strongly attenuated in miR-155-deficient mice as quantified by fluorescent intensity. Mice were intravenously injected with a fluorescent-labeled antibody against ICAM-1 4 hours after intraperitoneal injection of TNF- $\alpha$ , and adhesion molecule expression in mesenteric venules was visualized using intravital imaging (n=6). **G** through **I**, AGTR1 protein expression was decreased after miR-155 overexpression and enriched if miR-155 was inhibited in murine ECs (n=6). **J** and **K**, Murine ECs were simultaneously transfected with either pre-miR-155 or anti-miR-155 and the corresponding control compounds, and the respective AGTR1 3' untranslated region (UTR) or control construct and Firefly luciferase activity was normalized to Renilla luciferase activity. Relative AGTR1 3' UTR activity decreased after miR-155 overexpression and increased under miR-155 inhibition (n=6). **L** and **M**, Silencing of AGTR1 in murine ECs resulted in an increased expression of ICAM-1, as well as VCAM-1 (n=6). **N** and **O**, Concomitant knockdown of miR-155 and AGTR1 reversed the effect of single miR-155 inhibition on protein expression of ICAM-1, as well as VCAM-1 (n=6). Data represent mean values with SEM. \* $P < 0.05$  vs the corresponding control. #Bonferroni corrected level of significance  $< 0.05$  vs the corresponding group.

by miR-155 cannot be excluded (Table V in the online-only Data Supplement), our findings provide direct evidence that AGTR1 functions as a proangiogenic stimulator downstream of miR-155. This is in good correspondence with a recent report by Zhu et al<sup>11</sup> that had already shown a downregulation of AGTR1 and a decreased expression of vascular cell adhesion molecule 1, MCP-1, and *FLT-1* in response to angiotensin II in human umbilical vein ECs that overexpressed miR-155.

Following these conclusive in vitro results, we were surprised to detect a strong impairment of blood flow recovery at 14 days after femoral ligation in miR-155-deficient mice in vivo, contradictory to our in vitro findings. This defective phenotype is still detectable at 4 weeks, demonstrating that not only the time course but also the maximum extent of neovascularization is attenuated in miR-155-deficient mice. Histologic analysis led to the elucidation of this unexpected observation, because we detected a lower number of perivascular leukocytes after the induction of hindlimb ischemia. The critical importance of this infiltrating cell population as a source for proarteriogenic cytokines and growth factors is well documented,<sup>33</sup> and several reports directly correlated the number of perivascular macrophages with the rate of blood flow recovery.<sup>14,34</sup> Although these terminally differentiated cells are not directly incorporated in the growing vessels, they generate an inflammatory environment that allows the remodeling of pre-existing anastomoses to functional collateral arteries.<sup>2</sup> Among the secreted factors, TNF- $\alpha$  has a direct stimulatory role on collateral artery growth,<sup>13</sup> whereas macrophage-derived chemoattractants and growth factors stimulate further cell infiltration and vascular smooth muscle and EC proliferation. Indeed, the expression level of TNF- $\alpha$  was significantly lower in the hindlimb tissue of miR-155-deficient mice in comparison with wild-type controls, suggesting a potential impairment in arteriogenic cytokine production. Although the absolute number of circulating monocytes does not differ at baseline, we found a significantly lower increase in the absolute number of circulating monocytes after the induction of hindlimb ischemia as compared with wild-type animals. Interestingly, the number of the proinflammatory Ly6C<sup>hi</sup> subset is especially reduced at day 14 after femoral artery ligation, whereas the absolute number of Ly6C<sup>low</sup> monocytes does not differ between the strains, suggesting an alteration of the circulating monocyte composition. These findings are in good correspondence with a recent publication of Du et al,<sup>35</sup> which showed a reduced Ly6C<sup>hi</sup> monocyte subset in the spleen of global miR-155-deficient mice on an APOE<sup>-/-</sup> background. However, Donners et al<sup>36</sup> recently found a different result with significantly less Ly6C<sup>hi</sup> monocytes in the blood lymphocyte profile of mice with an exclusive deficiency of miR-155 in the hematopoietic system. A possible explanation for this discrepancy is that Donners et al<sup>36</sup> obtained their results in a model of chronic hyperlipidemia and exclusive hematopoietic miR-155 deficiency, whereas our model of femoral artery ligation represents an acute inflammatory stimulus in globally miR-155-deficient animals.

Following this notion that miR-155 in infiltrating cells is necessary for adaptive collateral artery growth, chimeric animals lacking miR-155 exclusively in the hematopoietic

system showed a virtually identical defective phenotype in blood flow restoration as the ubiquitous knockout. However, reconstitution of miR-155<sup>+/+</sup> BMCs in global miR-155<sup>-/-</sup> mice was not sufficient to rescue the defective phenotype, indicating a contribution of miR-155 expression in other cell populations. Our data show that miR-155 regulates adhesion molecule expression in murine ECs in vitro and in vivo by suppressing AGTR1, thereby promoting proarteriogenic endothelial properties and simultaneously suppressing angiogenesis via the same target gene, demonstrating that miR-155 expression in bone marrow-derived and nonhematopoietic cells is a mandatory prerequisite for effective arteriogenesis in vivo.

Our functional characterization of leukocyte-endothelial interaction and migration in miR-155-deficient mice revealed a significant impairment in these initiating steps of collateral artery growth, conclusively explaining the lower perivascular cell count in the hindlimb ischemia model. Previous studies in different neoplastic and progenitor cell populations had shown both positive<sup>37</sup> and negative<sup>38</sup> effects of miR-155 on migration, suggesting a cell-type-specific effect. Although our intravital imaging results do not differentiate between the individual leukocyte subpopulations, our in vitro characterization of a pure BMDM culture clearly demonstrates that the migratory capacity of this important proarteriogenic cell type depends on an intact function of miR-155. In addition, our PCR array-based comparison of miR-155-deficient BMDMs and wild-type cells yield a profound alteration of proarteriogenic cytokine expression after inflammatory activation. MCP-1 not only serves as a chemoattractant for subsequent circulating cell infiltration but also as a direct stimulus for vascular smooth muscle cell proliferation<sup>39</sup> and arterial remodeling. Our findings are in good correspondence with the recent report by Nazari-Jahantigh et al,<sup>40</sup> describing miR-155 as a key player in chemokine/cytokine production capacity of BMDMs in arteriosclerotic vascular disease. However, because none of the regulated proarteriogenic mediators in our study include a direct miR-155 binding site, the question of the direct target gene mediating these effects remained unknown. We focused on SOCS-1 as a potential mediator, after comparing the expression of 84 miR-155 target genes between wild-type and miR-155<sup>-/-</sup> macrophages. SOCS-1 is a well-documented endogenous inhibitor of the inflammatory response to injury, and SOCS-1-deficient mice die within 3 weeks of birth because of a severe generalized inflammatory reaction, characterized by macrophage infiltration of major organs<sup>41–43</sup> and a sustained increase in TNF- $\alpha$  expression.<sup>44</sup> The SOCS-1 mRNA includes a highly conserved binding site for miR-155, and the expressional repression of SOCS-1 by this miRNA was shown recently to contribute to tumor-associated inflammation in breast cancer<sup>45</sup> and antiviral immunity.<sup>46</sup> Our own data now show that SOCS-1 knockdown reverses the effects of miR-155 deficiency on proarteriogenic cytokine production, demonstrating that suppression of SOCS-1 is sufficient for the mediation of this proarteriogenic macrophage phenotype. Based on these findings, we propose a model of cell-specific divergent miRNA function on the different forms of vascular growth,



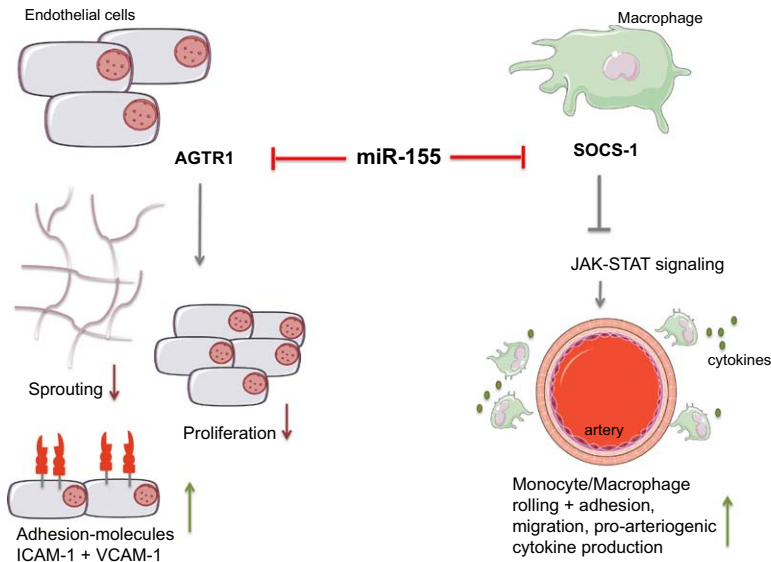


**Figure 8.** Model of cell-specific divergent and target gene-dependent microRNA miR-155 function on the different forms of vascular growth. Although miR-155 exerts cell-intrinsic antiangiogenic but proarteriogenic effects in endothelial cells (ECs) via suppression of AGTR1, proarteriogenic functions in monocytes and macrophages are mediated via the modulation of SOCS-1.

which depends on the relative expression of its direct target genes (Figure 8). Although miR-155 exerts cell-intrinsic antiangiogenic but proinflammatory effects in ECs via suppression of AGTR1, proarteriogenic functions are mediated via modulation of the leukocyte-enriched feedback regulator SOCS-1 in monocytes/macrophages.

Because most studies on the modulation of blood vessel growth by miRNAs showed synergistic effects on angiogenesis and arteriogenesis,<sup>5,7</sup> our findings of a divergent function of miR-155 on both forms are somewhat surprising. However, the 2 forms of vascular growth greatly differ with regard to stimuli, mediators, and regulatory principles,<sup>47</sup> and a stimulatory influence of an individual protein or RNA mediator on one process does not necessarily predict the effect on the other. In fact, van Solingen et al<sup>48</sup> recently showed that silencing of miR-126 by antagomir treatment impaired angiogenesis but not arteriogenesis after femoral artery ligation in mice. In this animal model the growth of capillaries alone cannot compensate for the occlusion of a major arterial vessel,<sup>47</sup> and blood flow restoration is predominantly dependent on arteriogenesis and not angiogenesis.<sup>47</sup> Our findings in miR-155-deficient mice are in good agreement with this concept, where the enlarged remodeling of arterial vessels in the proximal limb is the determinant for a sufficient perfusion of the downstream tissue.

The potential therapeutic inhibition or overexpression of miR-155 is hampered by its complex multifunctional role in basic immunity and its oncogenic potential, and, therefore, miR-155 is currently not a likely candidate for a potential clinical modulation of neovascularization. However, our findings demonstrate that miRNAs could represent promising targets for the control of a specific form of vascular growth, allowing, for example, the therapeutic stimulation of collateral artery growth in peripheral vascular disease without potential unwanted proangiogenic adverse effects on diabetic retinopathy, intraplaque angiogenesis, or tumor growth.

In addition, our findings further support the predominant dependency of blood flow reconstitution in vascular occlusive

disease in vivo on the compensatory growth of collateral arterial blood vessels over capillary proliferation. Mechanistically, our results demonstrate again that great caution is warranted in the extrapolation of miRNA studies performed in isolated cell populations to the in vivo situation.

## Acknowledgments

We thank Caterina Jaenich for expert technical assistance.

## Sources of Funding

This study is supported by the Deutsche Forschungsgemeinschaft, Germany, to Dr Grundmann (GR 3459/2-1) and Dr Moser (Mo 973/5-1 and 6-1) and by the Else Kroener-Fresenius-Stiftung to Dr Grundmann (2011\_A191). Dr Zeiser is supported by ZE 872/3-1 and Z2 in SFB850.

## Disclosures

None.

## References

1. Carmeliet P. Mechanisms of angiogenesis and arteriogenesis. *Nat Med*. 2000;6:389–395. doi: 10.1038/74651.
2. Heil M, Schaper W. Influence of mechanical, cellular, and molecular factors on collateral artery growth (arteriogenesis). *Circ Res*. 2004;95:449–458. doi: 10.1161/01.RES.0000141145.78900.44.
3. Ambros V. The functions of animal microRNAs. *Nature*. 2004;431:350–355. doi: 10.1038/nature02871.
4. Yang WJ, Yang DD, Na S, Sandusky GE, Zhang Q, Zhao G. Dicer is required for embryonic angiogenesis during mouse development. *J Biol Chem*. 2005;280:9330–9335. doi: 10.1074/jbc.M413394200.
5. Bonauer A, Carmona G, Iwasaki M, Mione M, Koyanagi M, Fischer A, Burchfield J, Fox H, Doebele C, Ohtani K, Chavakis E, Potente M, Tjwa M, Urbich C, Zeiher AM, Dimmeler S. MicroRNA-92a controls angiogenesis and functional recovery of ischemic tissues in mice. *Science*. 2009;324:1710–1713. doi: 10.1126/science.1174381.
6. Doebele C, Bonauer A, Fischer A, Scholz A, Reiss Y, Urbich C, Hofmann WK, Zeiher AM, Dimmeler S. Members of the microRNA-17–92 cluster exhibit a cell-intrinsic antiangiogenic function in endothelial cells. *Blood*. 2010;115:4944–4950.
7. Grundmann S, Hans FP, Kinniry S, Heinke J, Helbing T, Bluhm F, Sluijter JP, Hoefler I, Pasterkamp G, Bode C, Moser M. MicroRNA-100 regulates neovascularization by suppression of mammalian target of rapamycin in endothelial and vascular smooth muscle cells. *Circulation*. 2011;123:999–1009. doi: 10.1161/CIRCULATIONAHA.110.000323.

8. Liu Z, Yang D, Xie P, Ren G, Sun G, Zeng X, Sun X. MiR-106b and MiR-15b modulate apoptosis and angiogenesis in myocardial infarction. *Cell Physiol Biochem*. 2012;29:851–862. doi: 10.1159/000258197.
9. Liu LZ, Li C, Chen Q, Jing Y, Carpenter R, Jiang Y, Kung HF, Lai L, Jiang BH. Mir-21 induced angiogenesis through AKT and ERK activation and HIF-1 $\alpha$  expression. *PLoS One*. 2011;6:e19139.
10. van Mil A, Grundmann S, Goumans MJ, Lei Z, Oerlemans MI, Jaksani S, Doevendans PA, Sluijter JP. MicroRNA-214 inhibits angiogenesis by targeting Quaking and reducing angiogenic growth factor release. *Cardiovasc Res*. 2012;93:655–665. doi: 10.1093/cvr/cvs003.
11. Zhu N, Zhang D, Chen S, Liu X, Lin L, Huang X, Guo Z, Liu J, Wang Y, Yuan W, Qin Y. Endothelial enriched microRNAs regulate angiotensin II-induced endothelial inflammation and migration. *Atherosclerosis*. 2011;215:286–293. doi: 10.1016/j.atherosclerosis.2010.12.024.
12. Herr D, Rodewald M, Fraser HM, Hack G, Konrad R, Kreienberg R, Wulff C. Regulation of endothelial proliferation by the renin-angiotensin system in human umbilical vein endothelial cells. *Reproduction*. 2008;136:125–130. doi: 10.1530/REP-07-0374.
13. Hoefer IE, van Royen N, Rectenwald JE, Bray EJ, Abouhamze Z, Moldawer LL, Voskuil M, Piek JJ, Buschmann IR, Ozaki CK. Direct evidence for tumor necrosis factor- $\alpha$  signaling in arteriogenesis. *Circulation*. 2002;105:1639–1641.
14. Grundmann S, Hoefer I, Ulusans S, van Royen N, Schirmer SH, Ozaki CK, Bode C, Piek JJ, Buschmann I. Anti-tumor necrosis factor- $\alpha$  therapies attenuate adaptive arteriogenesis in the rabbit. *Am J Physiol Heart Circ Physiol*. 2005;289:H1497–H1505. doi: 10.1152/ajpheart.00959.2004.
15. Friedman RC, Farh KK, Burge CB, Bartel DP. Most mammalian mRNAs are conserved targets of microRNAs. *Genome Res*. 2009;19:92–105. doi: 10.1101/gr.082701.108.
16. Grimson A, Farh KK, Johnston WK, Garrett-Engle P, Lim LP, Bartel DP. MicroRNA targeting specificity in mammals: determinants beyond seed pairing. *Mol Cell*. 2007;27:91–105. doi: 10.1016/j.molcel.2007.06.017.
17. Lewis BP, Burge CB, Bartel DP. Conserved seed pairing, often flanked by adenosines, indicates that thousands of human genes are microRNA targets. *Cell*. 2005;120:15–20. doi: 10.1016/j.cell.2004.12.035.
18. Betel D, Koppal A, Agius P, Sander C, Leslie C. Comprehensive modeling of microRNA targets predicts functional non-conserved and non-canonical sites. *Genome Biol*. 2010;11:R90. doi: 10.1186/gb-2010-11-8-r90.
19. Betel D, Wilson M, Gabow A, Marks DS, Sander C. The microRNA.org resource: targets and expression. *Nucleic Acids Res*. 2008;36(database issue):D149–D153. doi: 10.1093/nar/gkm995.
20. Enright AJ, John B, Gaul U, Tuschl T, Sander C, Marks DS. MicroRNA targets in *Drosophila*. *Genome Biol*. 2003;5:R1. doi: 10.1186/gb-2003-5-1-r1.
21. Lee DY, Deng Z, Wang CH, Yang BB. MicroRNA-378 promotes cell survival, tumor growth, and angiogenesis by targeting SuFu and Fus-1 expression. *Proc Natl Acad Sci USA*. 2007;104:20350–20355. doi: 10.1073/pnas.0706901104.
22. Khorram O, Han G, Bagherpour R, Magee TR, Desai M, Ross MG, Chaudhri AA, Toloubeidokhti T, Pearce WJ. Effect of maternal under-nutrition on vascular expression of micro and messenger RNA in newborn and aging offspring. *Am J Physiol Regul Integr Comp Physiol*. 2010;298:R1366–R1374. doi: 10.1152/ajpregu.00704.2009.
23. Jiang L, Lin C, Song L, Wu J, Chen B, Ying Z, Fang L, Yan X, He M, Li J, Li M. MicroRNA-30e promotes human glioma cell invasiveness in an orthotopic xenotransplantation model by disrupting the NF- $\kappa$ B/I $\kappa$ B negative feedback loop. *J Clin Invest*. 2012;122:33–47.
24. Siragam V, Rutnam ZJ, Yang W, Fang L, Luo L, Yang X, Li M, Deng Z, Qian J, Peng C, Yang BB. MicroRNA miR-98 inhibits tumor angiogenesis and invasion by targeting activin receptor-like kinase-4 and matrix metalloproteinase-11. *Oncotarget*. 2012;3:1370–1385.
25. Greco S, De Simone M, Colussi C, Zaccagnini G, Fasanaro P, Pescatori M, Cardani R, Perbellini R, Isaia E, Sale P, Meola G, Capogrossi MC, Gaetano C, Martelli F. Common micro-RNA signature in skeletal muscle damage and regeneration induced by Duchenne muscular dystrophy and acute ischemia. *FASEB J*. 2009;23:3335–3346. doi: 10.1096/fj.08-128579.
26. Khudayberdiev S, Fiore R, Schrat G. MicroRNA as modulators of neuronal responses. *Commun Integr Biol*. 2009;2:411–413.
27. Liu T, Shen D, Xing S, Chen J, Yu Z, Wang J, Wu B, Chi H, Zhao H, Liang Z, Chen C. Attenuation of exogenous angiotensin II stress-induced damage and apoptosis in human vascular endothelial cells via microRNA-155 expression. *Int J Mol Med*. 2013;31:188–196. doi: 10.3892/ijmm.2012.1182.
28. O'Connell RM, Taganov KD, Boldin MP, Cheng G, Baltimore D. MicroRNA-155 is induced during the macrophage inflammatory response. *Proc Natl Acad Sci USA*. 2007;104:1604–1609. doi: 10.1073/pnas.0610731104.
29. Wei Y, Nazari-Jahanmogh M, Chan L, Zhu M, Heyll K, Corbalán-Campos J, Hartmann P, Thiemann A, Weber C, Schober A. The microRNA-342-5p fosters inflammatory macrophage activation through an Akt1- and microRNA-155-dependent pathway during atherosclerosis. *Circulation*. 2013;127:1609–1619. doi: 10.1161/CIRCULATIONAHA.112.000736.
30. Faraoni I, Antonetti FR, Cardone J, Bonmassar E. miR-155 gene: a typical multifunctional microRNA. *Biochim Biophys Acta*. 2009;1792:497–505. doi: 10.1016/j.bbdis.2009.02.013.
31. Martin MM, Buckenberger JA, Jiang J, Malana GE, Nuovo GJ, Chotani M, Feldman DS, Schmittgen TD, Elton TS. The human angiotensin II type 1 receptor +1166 A/C polymorphism attenuates microRNA-155 binding. *J Biol Chem*. 2007;282:24262–24269. doi: 10.1074/jbc.M701050200.
32. Roitbak T, Bragina O, Padilla JL, Pickett GG. The role of microRNAs in neural stem cell-supported endothelial morphogenesis. *Vasc Cell*. 2011;3:25. doi: 10.1186/2045-824X-3-25.
33. Schaper W, Scholz D. Factors regulating arteriogenesis. *Arterioscler Thromb Vasc Biol*. 2003;23:1143–1151. doi: 10.1161/01.ATV.0000069625.11230.96.
34. van Royen N, Hoefer I, Böttinger M, Hua J, Grundmann S, Voskuil M, Bode C, Schaper W, Buschmann I, Piek JJ. Local monocyte chemoattractant protein-1 therapy increases collateral artery formation in apolipoprotein E-deficient mice but induces systemic monocytic CD11b expression, neointimal formation, and plaque progression. *Circ Res*. 2003;92:218–225.
35. Du F, Yu F, Wang Y, Hui Y, Carnevale K, Fu M, Lu H, Fan D. MicroRNA-155 deficiency results in decreased macrophage inflammation and attenuated atherosclerosis in apolipoprotein E-deficient mice. *Arterioscler Thromb Vasc Biol*. 2014;34:759–767. doi: 10.1161/ATVBAHA.113.302701.
36. Donners MM, Wolfs IM, Stöger LJ, van der Vorst EP, Pöttgens CC, Heymans S, Schroen B, Gijbels MJ, de Winther MP. Hematopoietic miR155 deficiency enhances atherosclerosis and decreases plaque stability in hyperlipidemic mice. *PLoS One*. 2012;7:e35877. doi: 10.1371/journal.pone.0035877.
37. Liu J, van Mil A, Aguor EN, Siddiqi S, Vrijnsen K, Jaksani S, Metz C, Zhao J, Strijkers GJ, Doevendans PA, Sluijter JP. MiR-155 inhibits cell migration of human cardiac myocyte progenitor cells (hCMPCs) via targeting of MMP-16. *J Cell Mol Med*. 2012;16:2379–2386. doi: 10.1111/j.1582-4934.2012.01551.x.
38. Li S, Chen T, Zhong Z, Wang Y, Li Y, Zhao X. microRNA-155 silencing inhibits proliferation and migration and induces apoptosis by upregulating BACH1 in renal cancer cells. *Mol Med Rep*. 2012;5:949–954. doi: 10.3892/mmr.2012.779.
39. Parenti A, Bellik L, Brogelli L, Filippi S, Ledda F. Endogenous VEGF-A is responsible for mitogenic effects of MCP-1 on vascular smooth muscle cells. *Am J Physiol Heart Circ Physiol*. 2004;286:H1978–H1984. doi: 10.1152/ajpheart.00414.2003.
40. Nazari-Jahanmogh M, Wei Y, Noels H, Akhtar S, Zhou Z, Koenen RR, Heyll K, Gremse F, Kiessling F, Grommes J, Weber C, Schober A. MicroRNA-155 promotes atherosclerosis by repressing Bcl6 in macrophages. *J Clin Invest*. 2012;122:4190–4202. doi: 10.1172/JCI61716.
41. Naka T, Matsumoto T, Narazaki M, Fujimoto M, Morita Y, Ohsawa Y, Saito H, Nagasawa T, Uchiyama Y, Kishimoto T. Accelerated apoptosis of lymphocytes by augmented induction of Bax in SSI-1 (STAT-induced STAT inhibitor-1) deficient mice. *Proc Natl Acad Sci USA*. 1998;95:15577–15582.
42. Starr R, Metcalf D, Elefanti AG, Brysha M, Willson TA, Nicola NA, Hilton DJ, Alexander WS. Liver degeneration and lymphoid deficiencies in mice lacking suppressor of cytokine signaling-1. *Proc Natl Acad Sci USA*. 1998;95:14395–14399.
43. Kinjyo I, Hanada T, Inagaki-Ohara K, Mori H, Aki D, Ohishi M, Yoshida H, Kubo M, Yoshimura A. SOCS1/JAB is a negative regulator of LPS-induced macrophage activation. *Immunity*. 2002;17:583–591.
44. Morita Y, Naka T, Kawazoe Y, Fujimoto M, Narazaki M, Nakagawa R, Fukuyama H, Nagata S, Kishimoto T. Signals transducers and activators of transcription (STAT)-induced STAT inhibitor-1 (SSI-1)/suppressor of cytokine signaling-1 (SOCS-1) suppresses tumor necrosis factor  $\alpha$ -induced cell death in fibroblasts. *Proc Natl Acad Sci USA*. 2000;97:5405–5410. doi: 10.1073/pnas.090084797.
45. Jiang S, Zhang HW, Lu MH, He XH, Li Y, Gu H, Liu MF, Wang ED. MicroRNA-155 functions as an OncomiR in breast cancer by targeting the suppressor of cytokine signaling 1 gene. *Cancer Res*. 2010;70:3119–3127. doi: 10.1158/0008-5472.CAN-09-4250.

46. Wang P, Hou J, Lin L, Wang C, Liu X, Li D, Ma F, Wang Z, Cao X. Inducible microRNA-155 feedback promotes type I IFN signaling in antiviral innate immunity by targeting suppressor of cytokine signaling 1. *J Immunol*. 2010;185:6226–6233. doi: 10.4049/jimmunol.1000491.
47. Buschmann I, Schaper W. Arteriogenesis versus angiogenesis: two mechanisms of vessel growth. *News Physiol Sci*. 1999;14:121–125.
48. van Solingen C, Seghers L, Bijkerk R, Duijs JM, Roeten MK, van Oeveren-Rietdijk AM, Baelde HJ, Monge M, Vos JB, de Boer HC, Quax PH, Rabelink TJ, van Zonneveld AJ. Antagomir-mediated silencing of endothelial cell specific microRNA-126 impairs ischemia-induced angiogenesis. *J Cell Mol Med*. 2009;13(8A):1577–1585. doi: 10.1111/j.1582-4934.2008.00613.x.

### CLINICAL PERSPECTIVE

Following the narrowing or occlusion of an arterial vessel during the progression of coronary or peripheral artery disease, the organism can respond with the adaptive growth of new capillaries (angiogenesis) and collateral arteries (arteriogenesis). Although these mechanisms are protective in vascular occlusive disease, they can be harmful in the pathogenesis of other diseases, such as neoplastic tumor growth. In addition, in a clinical setting it can be desirable to selectively stimulate one form of vascular growth, for example, the enlargement of collateral arteries in peripheral artery disease without stimulating angiogenesis-driven processes, such as diabetic retinopathy or intraplaque angiogenesis. In this article we provide evidence that microRNA miR-155 exerts a proarteriogenic but antiangiogenic effect in a mouse model of peripheral artery disease. MiRs are short endogenous RNA molecules with an important regulatory function in many biological processes. The surprising divergent effect of miR-155 on the different forms of vascular growth depends on the cell-specific expression pattern of divergent target genes in endothelial cells and monocytes/macrophages. Our findings also show that blood flow reconstitution in our model of arterial occlusive disease is predominantly dependent on arteriogenesis. Because miRNA expression can be therapeutically targeted by oligonucleotide-based therapies, these regulatory RNAs could be promising targets for the independent therapeutic modulation of the different forms of vascular growth. However, because miR-155 exerts a multifunctional role in basic immunity, future studies will need to explore possible harmful adverse effects and other potential miRNA modulators for clinical application.

## MicroRNA-155 Exerts Cell-Specific Antiangiogenic but Proarteriogenic Effects During Adaptive Neovascularization

Franziska Pankratz, Xavier Bemtgen, Robert Zeiser, Franziska Leonhardt, Sheena Kreuzaler, Ingo Hilgendorf, Christian Smolka, Thomas Helbing, Imo Hoefer, Jennifer S. Esser, Max Kustermann, Martin Moser, Christoph Bode and Sebastian Grundmann

*Circulation*. 2015;131:1575-1589; originally published online April 7, 2015;  
doi: 10.1161/CIRCULATIONAHA.114.014579

*Circulation* is published by the American Heart Association, 7272 Greenville Avenue, Dallas, TX 75231

Copyright © 2015 American Heart Association, Inc. All rights reserved.

Print ISSN: 0009-7322. Online ISSN: 1524-4539

The online version of this article, along with updated information and services, is located on the World Wide Web at:

<http://circ.ahajournals.org/content/131/18/1575>

Data Supplement (unedited) at:

<http://circ.ahajournals.org/content/suppl/2015/04/07/CIRCULATIONAHA.114.014579.DC1.html>

**Permissions:** Requests for permissions to reproduce figures, tables, or portions of articles originally published in *Circulation* can be obtained via RightsLink, a service of the Copyright Clearance Center, not the Editorial Office. Once the online version of the published article for which permission is being requested is located, click Request Permissions in the middle column of the Web page under Services. Further information about this process is available in the [Permissions and Rights Question and Answer](#) document.

**Reprints:** Information about reprints can be found online at:

<http://www.lww.com/reprints>

**Subscriptions:** Information about subscribing to *Circulation* is online at:

<http://circ.ahajournals.org/subscriptions/>



## **Supplemental material**

### **A) Supplementary methods**

### **B) Supplementary tables**

1. Primer sequences and antibodies.
2. Results of PCR array “MiR-155 targets” comparing murine wildtype to miR-155 deficient endothelial cells (ECs).
  - A) Genes enriched in miR-155<sup>-/-</sup> ECs vs. wildtype ECs
  - B) Genes downregulated in miR-155<sup>-/-</sup> ECs vs. wildtype ECs
3. Results of PCR array “Inflammatory cytokines and receptors” BMDM.
  - A) Genes enriched in miR-155<sup>-/-</sup> BMDM vs. wildtype BMDM
  - B) Genes downregulated in miR-155<sup>-/-</sup> BMDM vs. wildtype BMDM
4. Results of PCR array “MiR-155 targets” comparing murine wildtype to miR-155 deficient bone marrow derived macrophages (BMDM).
  - A) Genes enriched in miR-155<sup>-/-</sup> BMDM vs. wildtype BMDM
  - B) Genes downregulated in miR-155<sup>-/-</sup> BMDM vs. wildtype BMDM
5. Results of PCR array “Mouse angiogenesis”: Comparison of wildtype and miR-155 deficient murine ECs.
  - (A) Genes enriched in miR-155<sup>-/-</sup> ECs.
  - (B) Genes downregulated in miR-155<sup>-/-</sup> ECs.

### **C) Supplementary figures**

1. MiR-155 expression in murine ECs under hypoxic conditions.
2. MiR-155 transfection efficacy and viability following transfection procedure in human ECs.
3. Silencing efficacy of AGTR1 in human and murine ECs.
4. Purity of isolated and cultured murine BMDM.
5. Baseline blood leukocyte count in wildtype and miR-155 deficient mice.
6. Phenotypic characterization of monocytes in wildtype and miR-155 deficient mice.
7. SOCS-1 silencing efficacy in BMDM using RNA interference.
8. Bone marrow cell transplantation efficacy in mice.

## **Supplementary methods**

### **Cell culture**

Human umbilical vein endothelial cells (HUVECs) were isolated from donated umbilical cords and cultivated in endothelial basal medium supplemented with EGF single quotes (PELOBiotech GmbH, Martinsried, Germany) and 10% FBS and used until passage five.

Murine C166 ECs were cultured in Dulbecco`s Modified Eagle Medium (DMEM), Life technologies, Darmstadt, Germany, supplemented with 10% FBS.

For culturing of mice bone marrow derived macrophages (BMDM), bone marrow cells were either isolated out of the femur bone of wildtype or miR-155 deficient mice and plated in 6 well plates ( $1 \times 10^6$  cells per well) in RPMI media supplemented with 10% FBS, 1% non-essential amino acids and 2% penicillin/streptomycin (all Life technologies, Darmstadt, Germany). Bone marrow cells were differentiated to macrophages by stimulation with 30ng/ml of monocyte colony stimulating factor number 1 (MCSF-1) for three days. To confirm the successful differentiation, cells were analyzed for expression of the macrophage marker F4/80 by flow cytometry (Supplementary figure 5) using RPE-conjugated antibodies against F4/80 and corresponding negative control IgG2b (for further information please refer to supplementary table 1) using a FACSCalibur (BD Biosciences, Franklin Lakes, NJ, USA) .

### **Transfection**

For microRNA transfection, cells were cultured to 70% of confluence and transfected with 5nM precursor (premiR-155) or 10nM antisense (antimiR-155) oligonucleotides or the corresponding control compounds (premiR-cont./antimiR-cont.) using Lipofectamin RNAiMax (all Life technologies, Darmstadt, Germany) according to the manufacturer`s instructions. For transfection efficacy please refer to Supplementary figure 1.

For silencing of SOCS-1 or AGTR1 BMDM, HUVECs or murine C166 ECs were grown to 80% of confluence and cells were transfected with 20nmol of either a combination of two small interfering (si) RNAs against SOCS-1 or AGTR1 or the corresponding control

compound, siRNA-Cont. (all Life technologies). For silencing efficacy please refer to Supplementary figure 3+8.

### **Taqman-based stem-loop PCR for microRNA-expression and real-time PCR for mRNA-expression analysis**

MicroRNA expression was validated by quantitative stem-loop PCR technology (TaqMan MicroRNA Assays, Life technologies, Darmstadt, Germany) as previously described<sup>1</sup>. The use of target-specific reverse transcription primers and TaqMan hybridization probes allowed the specific detection of mature microRNAs. MicroRNA expression was normalized to the expression of the small RNA rnu19.

For quantitative analysis of mRNA-levels up to 1µg total RNA was transcribed to cDNA (iScript, BioRad, München, Germany) and real-time PCR was performed on a MyIQ cycler (BioRad) as previously described<sup>2</sup>. The expression of mRNA was normalized to human RNA polymerase II (hrpII). For primer sequences please refer to supplementary table 1.

### **MTT viability assay**

To exclude direct toxic effects of pre- and antimiR transfection procedure, cellular viability was assessed at six hours after transfection of HUVECs by measuring the metabolization of MTT [3-(4,5-dimethylthiazol-2-yl)-2,5-diphenyl-2H-tetrazolium bromide]. HUVECs were cultured in 6 well plates and six hours after transfection 5mg/ml MTT (Sigma Aldrich, St. Louis, MO, USA) was added and cells were cultured for additional three hours before adding 2.5ml of MTT solvent (4mM HCL, 0.1% Igepal CA-630 in isopropanol). Samples were transferred in triplicates in a 96 well plate and absorbance was measured in plate reader at 590nm with reference filter set at 620nm.

### **Proliferation assay**

Proliferation of HUVECs transfected with either premiR-155 or antimiR-155 oligonucleotides

or the respective control compounds was determined by measuring the metabolization of MTT [3-(4,5-dimethylthiazol-2-yl)-2,5-diphenyl-2H-tetrazolium bromide]. Transfected cells were cultured in 6 well plates for 36 hours before adding 5mg/ml MTT (Sigma Aldrich, St. Louis, MO, USA) and assay was performed as described above.

### **Apoptosis and cell viability assay**

Apoptosis and cell viability were examined in wildtype and miR-155 deficient BMDM using the ApoTox-Glo™ Triplex assay from Promega, Madison, WI, USA, according to manufacturer's instructions. This assay allowed the simultaneously quantification of live-cell protease activity and caspase-3 and -7 activities.

### **Luciferase Assay**

Cells were plated in a 96 well plate and cultured to 70% of confluence and either transfected with 50ng AGTR1-3'UTR plasmid or the corresponding control plasmid (all GeneCopoeia™/tebu-bio, Le Perray-en-Yvelines Cedex, France), both containing the firefly luciferase gene from *photinus pyralis* as well as the renilla gene from *renilla reniformis* and with miR-155 specific precursor (premiR-155) or antisense oligonucleotides (antimiR-155) or the respective control compounds (premiR-cont./antimiR-cont.). 24 hours following transfection Dual-Glow-luciferase assay (GeneCopoeia™) was performed according to manufacturer's instructions using a Glomax, 96 microplate luminometer from Promega Madison, WI, USA and obtained firefly activity was normalized to renilla activity.

### **Matrigel tube formation assay**

24 hours following microRNA transfection, the assay was performed at least three times as previously described<sup>3</sup>.



### **Aortic Ring assay**

Endothelial sprouting of aortic rings was measured using the aortic ring assay. Aortas were isolated from B6Cg-MiR-155<sup>tm1.1Rsky</sup>/J and C57/BL6J mice (12 weeks of age, male) and cut into little rings. Aortas were incubated overnight (37°C, 5% CO<sub>2</sub>) in Optimem (Life technologies, Darmstadt, Germany). Subsequently, aortic rings were embedded in collagen gel and stimulated on day zero, three and seven with bFGF (50ng/ml) in Optimem supplemented with 2.5% FBS and 2% penicillin/streptomycin (all Life technologies). Day seven represented the endpoint and aortic rings were fixed in 4% paraformaldehyde and subsequently stained overnight at 4°C using TOMATO-Lectin-FITC and anti-SMA-Cy3 antibody.

For silencing of AGTR1, siRNA was delivered to aortic ring tissue using Lipofectamine according to manufacturer's instructions and 24 hours following transfection aortic rings were embedded and protocol was performed as described above. Endpoint for transfected rings was day ten. Growth-factor-induced microvessels were counted by a blinded investigator and representative pictures were taken under a Leica TCS SP2 AOBS spectral confocal microscope (Leica Camera, Solms, Germany).

### **In vitro chemotaxis assay**

Chemotaxis of wildtype and miR-155<sup>-/-</sup> BMDM was measured using a modified Boyden chamber (5µm-pore polycarbonate filter in transwell chamber, Corning, Lowell, MA, USA). Recombinant murine MCP-1 (50ng/ml) was used as chemotaxis stimulant in the lower chamber and cells were allowed to migrate for three hours. Migrated cells were collected and counted in a Neubauer chamber.

### **PCR array "Inflammatory cytokines and receptors"**

Wildtype and miR-155<sup>-/-</sup> BMDM were cultured as described above and stimulated for 24 hours with 10ng/ml LPS and RNA was isolated using the miRNA isolation kit from Qiagen,

Hilden, Germany. The mouse PCR array “Inflammatory cytokines and receptors” (Qiagen, PAM-011Z) allowed the expression analysis of 84 key genes and was performed according to manufacturer’s instructions.

### **PCR array “MiR-155 targets”**

Murine endothelial and bone marrow cells were isolated out of wildtype and miR155<sup>-/-</sup> mice. Bone marrow cells were differentiated as described above, RNA was isolated and PCR array “Murine miR-155 targets (Qiagen, PAMM-6002Z) was performed according to manufacturer’s instructions.

### **PCR array “Angiogenesis”**

Murine endothelial cells were isolated out of wildtype and miR155<sup>-/-</sup> mice, RNA was isolated and PCR array “Angiogenesis” (Qiagen, PAMM-024Z) was performed according to manufacturer’s instructions.

### **Enzyme-linked immunosorbent assay (ELISA)**

The concentration of CCL2 (MCP-1), CCL12 (MCP-5) and CCL4 (MIP-1 beta) was determined in native protein lysates of LPS stimulated (10ng/ml, 24 hours) BMDM using a CCL2 and CCL4 ELISA kit from Preprotech, Hamburg, Germany and a CCL12 ELISA kit from R&D systems, Wiesbaden, Germany.

### **Mice**

C57/BL6J mice were purchased either from Charles River or from the local stock of the animal facility at University Hospital Freiburg, Germany. B6Cg-MiR-155<sup>tm1.1Rsky</sup>/J mice were obtained from the Jackson Laboratory and bred in a specific pathogen free animal facility of the University Hospital Freiburg. Male and female mice were used between three to twelve weeks of age for the different experiments. Animal protocols were approved by the

Regierungspraesidium Freiburg, Germany and all studies conformed to the Guide for the Care and Use of Laboratory Animals published by the directive 2010/63/EU of the European Parliament.

### **Mouse Matrigel plug assay**

Mouse Matrigel plug assay was performed as previously described<sup>4</sup>. In brief, 500µl Matrigel (BD Biosciences, Franklin Lakes, NJ, USA) was mixed with 1µl Heparin (100.000I.E., B. Braun, Melsungen, Germany) and subcutaneously (s.c.) injected into the abdominal flanks of male C57/BL6J and B6Cg-MiR-155<sup>tm1.1Rsky</sup>/J mice and 10 days following injection plugs were harvested, fixed in 4% PFA, paraffin-embedded and sectioned. Blood vessel infiltration was analyzed in three imaging fields per hematoxylin- and eosin-stained section by a blinded investigator.

### **Intravital imaging of mesenteric venules**

Intravital imaging of mesenteric venules was performed four hours after systemic treatment with TNF-alpha (10ng/g body weight) in C57/BL6J and B6Cg-MiR-155<sup>tm1.1Rsky</sup>/J male mice, three weeks of age, under anesthesia with ketamine (100mg/kg) and xylazine (2mg/kg). To visualize leukocytes, 60µl of fluorescent dye rhodamine 6G (1mg/ml, Sigma-Aldrich, St. Louis, MO, USA) were intravenously injected. An ileal loop was exteriorized through a midline incision in the abdominal wall and placed in a plastic dish to observe the peri-intestinal microcirculation in the mesentery by intravital imaging. Leukocyte-endothelium interaction was recorded for one minute in three veins per mouse. Afterwards a blinded investigator quantified the number of interacting cells. The determined diameter of examined venules was normalized to 100µm.

For the *in vivo* staining of endothelial adhesion molecules mice were i.v. injected with fluorescent antibodies against ICAM-1 (FITC-labeled 660ng per g body weight) as well as VCAM-1 (eFluor450-labeled, 330ng per g body weight, for detailed information please refer

to supplementary table 1) following TNF-alpha treatment. Rhodamine was not injected due to overlapping fluorescent spectrum with used antibodies. As negative control, antibodies were injected without prior TNF-alpha treatment. Staining was visualized by intravital imaging of mesenteric venules, as already described.

### **Peritonitis model**

For induction of sterile peritonitis twelve weeks old female C57/BL6J and B6Cg-MiR-155<sup>tm1.1Rsky</sup>/J mice were injected i.p. with 2ml of 4% thioglycollate (Sigma-Aldrich, St. Louis, MO, USA) and two days after injection mice were sacrificed by cervicooccipital dislocation and cells were recovered by peritoneal lavage with 6ml RPMI medium (Life technologies, Darmstadt, Germany) and counted by the central lab, University hospital Freiburg, Germany.

### **Phenotypic analysis of monocytes following hind limb ischemia in mice by flow cytometry**

Blood of C57/BL6J and B6Cg-MiR-155<sup>tm1.1Rsky</sup>/J mice was analyzed at day 0 for baseline characterization as well as at day 14 following femoral artery ligation.

For the differentiation between neutrophils, monocytes and further subdivision in Ly6C<sup>hi</sup> and Ly6C<sup>low</sup> monocytes cells were stained with anti-CD45.2, -CD115, -CD11b and -Ly6C antibodies and in addition staining mix also included antibodies against the surface marker CCR2, CD49d (VLA4), PSGL1 and CD62L (for detailed information please refer to supplementary table 1). Staining was performed for 30 minutes on ice. Total leukocyte count was determined under a Zeiss microscope (Oberkochen, Germany) using a Neubauer chamber.

For the staining of intracellular cytokines, cells were incubated at 37°C, 5% CO<sub>2</sub> in RPMI medium containing 1µg/ml LPS as well as 1µl/ml BD Golgi Plug™ and 0,6µl/ml BD Golgi STOP™ (both BD Biosciences) and antibodies against CD115, CD11b and CD45.2.

Following incubation, cells were fixed and permeabilized using cytofix/cytoperm (BD Biosciences) and stained for 45 minutes on ice with antibodies against IL-10, MCP-1, TNF- $\alpha$  as well as IL-6 (for detailed antibody information, please refer to supplementary table 1). Flow cytometry measurements were done with the FACS Canto II (BD Biosciences, Franklin Lakes, NJ, USA) and data analysis was performed using the FlowJo software and all results were normalized to corresponding fmo control.

### **Generation of chimeric mice**

For transplantation experiments, recipient wildtype or miR155<sup>-/-</sup> mice were lethally irradiated (two times at interval of four hours, 5Gy) and in between these intervals bone marrow cells of donor wildtype or miR155<sup>-/-</sup> mice were isolated out of the thigh bone. Recipients were intravenously injected (i.v.) with  $5 \times 10^6$  cells suspended in 100 $\mu$ l buffered saline solution. Eight weeks after transplantation, hindlimb ischemia operation was performed on these mice, as described above.

### **Transplantation efficacy**

To test the transplant efficacy in transplantation experiments (Supplementary figure 7), protocol was performed as already described with recipient C57BL/6 luc mice positive for the T-Cell marker Thy1.1 and donor miR-155<sup>-/-</sup> mice positive for the T-Cell marker Thy1.2 (n=3). Eight weeks after transplantation circulating leukocytes were analyzed by flow cytometry (FACSCalibur, BD Biosciences, Franklin Lakes, NJ, USA) for the presence of Thy1.1 or Thy1.2 using corresponding antibodies (for further information please refer to supplementary table 1).

### **Immunohistology**

For immunohistology 5 $\mu$ m frozen tissue sections were processed as previously described<sup>5</sup>, incubated with the appropriate primary and secondary antibodies (for further information



please refer to supplementary table 1) and embedded in mowiol. Imaging was performed on a Zeiss Axioplan microscope and images were processed for contrast enhancement. For quantitative assessment, the number of CD11b positive cells per imaging field was counted in three randomly placed regions of interest in the adductor muscle.

**Supplementary table 1**

Primer sequences, antibodies, miRNA assays, vectors.

PCR Primers				
Gene	Species	Forward	Reverse	
AGTR1	human/ mouse	5´ TCAGCCAGCGTCAGTTTCAA 3´	5´ CTACAAGCATTGTGCGTCGAAG 3´	
CCL12	mouse	5´ CCACACTTCTATGCCTCCTG 3´	5´ ACAGGAGAATCACAAGCAGC 3´	
CCL2	mouse	5´ AGGTGTCCCAAAGAAGCTGTA 3´	5´ ATGTCTGGACCCATTCTTCT 3´	
CCL4	mouse	5´ TGTCTGCCCTCTCTCTCCTC 3´	5´GAGCAAGGACGCTTCTCAGT3´	
HRPII	human/ mouse	5´ GCACCACGTCCAATGACAT 3´	5´GTGCGGCTGCTTCCATAA3´	
SOCS-1	mouse	5´ GCAGCTCGAAGAGGCAGTCGAA 3´	5´ GCTCCCACTCTGATTACCGGCG 3´	
TNF-α	mouse	5´ ACCCCTTTATTGTCTACTCCTC 3´	5´GTCCCAGCATCTTGTGTTTC 3´	
Taqman Assay				
Assay name		Assay ID	Kit Part No.	Company
rnu19		001003	4440886	Life technologies
mmu-miR-155		00180	4440886	Life technologies
hsa-miR-155		002287	4440886	Life technologies
Primary antibodies				
Against	Host species	Clone ID	Company	(label)
CD11b	rat	M1/70.15	AbD Serotec	FITC
SMA	mouse	1A4	Sigma-Aldrich	FITC
SMA	mouse	1A4	Sigma-Aldrich	Cy3
AGTR1	rabbit	polyclonal	Abcam	
SOCS-1	goat	polyclonal	Abcam	

**Secondary antibodies**

<b>Against</b>	<b>Host species</b>	<b>Clone ID</b>	<b>Company</b>	<b>(label)</b>
rat	goat	polyclonal	Chemicon International	Cy3

**Staining reagents**

<b>Short name</b>	<b>Catalog No.</b>	<b>Full name</b>	<b>Company</b>	<b>(label)</b>
DAPI	D1306	4',6-Diamidin-2-phenylindol	Life technologies	
TOMATO Lectin	FL-1171	Fluorescein Lycopersicon Esculentum	Vector Laboratories	FITC

**FACS antibodies**

<b>Against</b>	<b>Host species</b>	<b>Clone ID</b>	<b>Company</b>	<b>(label)</b>
CD90.1	mouse	A20	BD Biosciences	FITC
CD90.2	rat	104	BioLegend	PE
F4/80	rat	Cl:A3-1	AbD Serotec	RPE
IgG2b rat	N/A	MCA1125	AbD Serotec	RPE
CD106	mouse	429	eBioscience	APC
CD54	rat	YN1/1.7.4	eBioscience	FITC
IgG1 mouse	N/A	679.1Mc7	Beckman Coulter	PE
IgG1 mouse	N/A	X40	BD Biosciences	APC
CD54	rat	YN1/1.7.4	eBioscience	FITC
CD106	rat	429	eBioscience	eFluor®450
Ly6C	rat	HK1.4	BioLegend	PE/Cy7
CD115	rat	AFS98	eBioscience	PE
CD49d	rat	R1-R2	eBioscience	eFluor® 710

Against	Host species	Clone ID	Company	(label)
CD62L	rat	MEL-14	BioLegend	PE/Cy7
CCR2	rat	475301	R&D systems	APC
CD11b	rat	M1/70	BioLegend	APC/Cy7
CD162	rat	2PH1	BD Biosciences	BV421™
CD45.2	mouse	104	BioLegend	BV510™
CCL2	armenian hamster	2H5	eBioscience	FITC
IL-10	rat	JES5-16E3	eBioscience	PerCP- Cy5.5.
IL-6	rat	MP5-20F3	BioLegend	APC
TNF-alpha	rat	MP6-XT22	BioLegend	BV421™
IgG1 mouse	N/A	MCA928F	AbD Serotec	FITC
Precursor and antisense oligonucleotides				
miRNA	Cat #	ID#	Company	
premiR-cont.	AM17110	N/A	Life technologies	
hsa premiR-155	AM17100	PM12601	Life technologies	
mmu premiR-155	AM17100	PM13058	Life technologies	
antimiR-cont.	AM17010	N/A	Life technologies	
hsa antimiR-155	AM17000	AM12601	Life technologies	
mmu antimiR-155	AM17000	AM13058	Life technologies	
siRNAs				
Against	Cat #	ID #	Company	
hsa AGTR1	10620318/19	219119B11	Life technologies	
		219119B12		

<b>Against</b>	<b>Cat #</b>	<b>ID #</b>	<b>Company</b>
mmu AGTR1	10620318/19	262248A04/05	Life technologies
		262248A06/07	
SOCS-1	10620318/19	205297D05	Life technologies
		205297D07	
Stealth™ RNAi	12935-400	N/A	Life technologies
negative control			
duplex			
<b>Vectors</b>	<b>Cat #</b>	<b>Reporter genes/ Promotor</b>	<b>Company</b>
3' UTR AGTR1	MmiT041699-	hLuc-hRluc	GeneCopoeia™
(pEZX-MT01)	MT01	SV40	
Negative control	CmiT000001-	hLuc-hRluc	GeneCopoeia™
vector	MT01	SV40	



**Supplementary table 2**

Results of PCR array “Murine miR-155 targets”. Comparison of miR-155 target gene expression levels in wildtype and miR155-/- endothelial cells (ECs).

(A) Genes enriched in miR155-/- ECs compared to wildtype ECs.

<b>Symbol</b>	<b>Gene name</b>	<b>Fold regulation</b>
Apc	AI047805	1,02
Zmym2	Zfp198	1,05
Chd9	1810014J18Rik	1,08
Det1	2610034H20Rik	1,12
Tle4	Bce-1	1,13
Stxbp5l	LLGL4	1,15
Tomm20	1810060K07Rik	1,15
Msh2	AI788990	1,19
Skiv2l2	2610528A15Rik	1,24
Mlh1	1110035C23Rik	1,25
Ttl	2410003M22Rik	1,26
Tceb1	2610043E24Rik	1,29
Usp14	2610005K12Rik	1,36
Msh6	Gtmbp	1,40
Lpar6	2610302I02Rik	1,67
Myb	c-myb	1,68
Zic3	Bn	1,82
Socs1	SOCS-1	2,06
Card11	BIMP3	2,06
Sec14l5	-	2,06
Rap1b	2810443E11Rik	2,69

<b>Symbol</b>	<b>Gene name</b>	<b>Fold regulation</b>
Inpp5d	SHIP-	3,17
Mafb	Kreisler	13,89
Tm6sf1	AI428514	17,46
Agtr1a	Agtr1	50,77
Sfpi1	PU.1	669,06

**Supplementary table 2**

(B) Genes downregulated in miR155-/- ECs compared to wildtype cells.

<b>Symbol</b>	<b>Gene name</b>	<b>Fold regulation</b>
Gdf6	BMP13	-49,66
Pam	PHM	-8,90
Bach1	6230421P05Rik	-8,60
Hivep2	Schnurri-2	-8,42
Ski	2310012I02Rik	-6,43
Zfp236	AI447957	-6,38
Ilf3	NF90	-5,95
Phf17	Jade1	-5,67
Stx16	5430410K23Rik	-5,44
Ldoc1	Gm366	-5,40
Zfp407	ZNF407	-4,90
Nova1	Nova-1	-4,74
Arid2	1700124K17Rik	-4,70
Runx2	AML3	-4,30
Edn1	ET-1	-4,12
Smad5	Madh5	-4,07
Cebpb	CRP2	-3,82
Smad1	Madh1	-3,59
Trp53inp1	Teap	-3,52
Nfatc2ip	NIP45	-3,28
Meis1	C530044H18Rik, Evi8	-3,00
Ets1	AI196000	-2,90
Csnk1g2	2810429I12Rik	-2,84

<b>Symbol</b>	<b>Gene name</b>	<b>Fold regulation</b>
Pea15a	Mat1	-2,47
Bcorl1	6720425J07Rik	-2,09
Dync1i1	DH IC-1	-2,08
Astn2	Astnl	-2,02
Fadd	FADD	-1,99
Rreb1	1110037N09Rik	-1,91
Ifngr1	Ifgr	-1,87
Ndfip1	0610010M22Rik	-1,78
Ikbke	IKK-i	-1,76
Aicda	Aid	-1,71
Sep 11	6230410I01Rik	-1,69
Tab2	Map3k7ip2	-1,67
Myo10	AW048724	-1,65
Mecp2	1 Mbd5	-1,62
Dhx40	PAD	-1,53
Sox1	BB176347	-1,49
Matr3	1110061A14Rik	-1,48
Pld5	B230365F16Rik	-1,46
Fgf7	Kgf	-1,43
Hnrnpa3	2410013L13Rik	-1,30
Zfp652	9530033F24Rik	-1,23
Peli1	2810468L03Rik	-1,22
Cyr61	CCN1	-1,19
Mef2a	A430079H05Rik	-1,18
Jarid2	jumonji	-1,18
G3bp2	AA409541	-1,15

<b>Symbol</b>	<b>Gene name</b>	<b>Fold regulation</b>
Ripk1	RIP	-1,14
Uqcr11	0710008D09Rik	-1,13
Rhoa	Arha2	-1,11
Tshz3	Tsh3	-1,10
Irak3	IRAK-M	-1,06
Aak1	5530400K14Rik	-1,04
Kras	Kras2	-1,01

**Supplementary table 3**

Results of PCR array “Inflammatory cytokines and receptors”: Comparison of wildtype bone marrow derived macrophages (BMDM) to miR-155-deficient BMDM.

(A) Genes enriched in miR-155-/- BMDM compared to wildtype cells.

<b>Symbol</b>	<b>Gene Name</b>	<b>Fold regulation</b>
Cxcl13	ANGIE2	45,25
Cxcl11	Cxc11	6,50
Cxcl5	GCP-2	2,51
Cxcr3	Cd183	2,16
Cxcr2	CD128	1,96
Ccr10	Gpr2	1,92
Il16	KIAA4048	1,88
Il10ra	Il10r	1,87
Pf4	Cxc20l4	1,80
Itgam	CD11b	1,73
Il13ra1	Il13ra	1,62
Il6st	CD130	1,56
Il1r1	CD121a	1,55
Il10rb	IL-10R2	1,53
Il6ra	CD126	1,49
Cxcl9	Mig	1,41
Mif	GIF	1,40
Tnfrsf1a	TNF-alphaR1	1,39
Tgfb1	TGF-beta1	1,39
Il1r2	CD121b	1,38
Ccr7	CD197	1,37
Tollip	4930403G24Rik	1,36

<b>Symbol</b>	<b>Gene Name</b>	<b>Fold regulation</b>
Il1b	IL-1beta	1,29
C3	HSE-MSF	1,28
Il4	Il-4	1,28
Ccr4	Cmkbr4	1,25
Ccl1	Tca-3	1,23
Ccl11	eotaxin	1,23
Ccr8	mCCR8	1,23
Crp	AI255847	1,23
Cxcl15	lungkine	1,23
Ifng	IFN-g	1,23
Il20	MGC130536	1,23
Il3	HCGF	1,23
Il5ra	CD125	1,23
Lta	TNF-beta	1,23
Cd40lg	CD154	1,23
Il1f6	IL1RP2	1,22
Ccr3	Cmkbr3	1,21
Cxcl1	Gro1	1,18
Aimp1	p43	1,16
Ccl19	MIP3B	1,15
Itgb2	Lfa1	1,15
Tnfrsf1b	TNTNF-a-R2	1,15
Il15	AI503618	1,15
Il2rb	CD122	1,14
Il1f8	2310043N20Rik	1,11
Cxcr5	Blr1	1,11



<b>Symbol</b>	<b>Gene Name</b>	<b>Fold regulation</b>
Il18	Ig1f, Il-18	1,10
Il17b	1110006O16Rik	1,05
Spp1	ETA-1	1,01

**Supplementary table 3**

(B) Genes downregulated in miR-155-deficient BMDM compared to wildtype BMDM.

<b>Symbol</b>	<b>Gene Name</b>	<b>Fold regulation</b>
Ccl17	Abcd-2	-3,73
Ccl12	MCP-5	-3,46
Ccl8	MCP-2	-3,12
Ccl20	MIP-3A	-2,62
Ccl2	MCP-1	-2,53
Ccl7	MCP-3	-2,53
Ccl4	MIP-1B	-2,45
Ccr2	Ccr2a	-1,88
Il10	Il-10	-1,80
Casp1	Il1bc	-1,61
Bcl5	Bcl5	-1,60
Ccl25	CKb15	-1,58
Ccl3	MIP 1-a	-1,51
Abcf1	Abc50	-1,49
Ccl22	ABCD-1	-1,48
Ccl5	RANTES	-1,48
Ccl6	MRP-1	-1,48
Ccr9	Cmkbr10	-1,36
Xcr1	Ccxcr1	-1,36
Ccl24	MPIF-2,	-1,31
Ccr1	Mip-1a-R	-1,30
Cxcl12	Sdf1	-1,16
Ccr5	CD195	-1,11
Ccr6	CCR-6	-1,11

<b>Symbol</b>	<b>Gene Name</b>	<b>Fold regulation</b>
Il2rg	CD132	-1,09
Ltb	p33	-1,09
Cx3cl1	CX3C	-1,07
Cxcl10	IP-10	-1,06
Il13	Il-13	-1,06
Ccl9	MRP-2	-1,05
Il1a	Il-1a	-1,04
Tnf	TNF-alpha	-1,04
Il11	IL-11	-1,03

**Supplementary table 4**

Results of PCR array “Murine miR-155 targets”. Comparison of miR-155 target gene expression levels in wildtype and miR155-/- BMDM.

(A) Genes enriched in miR155-/- BMDM compared to wildtype cells.

<b>Symbol</b>	<b>Gene name</b>	<b>Fold regulation</b>
Ma1b	Kreisler	1,06
Bach1	6230421P05Rik	1,08
Dync1i1	DH IC-1	1,17
Fadd	FADD	1,21
Arid2	1700124K17Rik	1,27
Msh2	AI788990	1,43
Tle4	Bce-1	1,47
Myo10	AW048724	1,55
Nfatc2ip	NIP45	1,57
Smad1	Madh1	1,60
Jarid2	jumonji	1,65
Sfpi1	PU.1	1,65
Apc	AI047805	1,82
Peli1	2810468L03Rik	1,91
Tab2	Map3k7ip2	2,04
Hivep2	Schnurri-2	2,10
Myb	c-myb	2,25
Phf17	Jade1	2,28
Ripk1	RIP	2,31
Csnk1g2	2810429I12Rik	2,89
Zfp407	ZNF407	2,93

<b>Symbol</b>	<b>Gene name</b>	<b>Fold regulation</b>
Irak3	IRAK-M	3,25
Trp53inp1	Teap	3,29
Runx2	AML3	3,97
Zfp236	AI447957	5,82
Foxo3	1110048B16Rik	6,87
Smad5	Madh5	6,96
Cebpb	CRP2	7,67
Stx16	5430410K23Rik	8,17
Ikbke	IKK-i	8,57
Chd9	1810014J18Rik	9,38
Bcorl1	6720425J07Rik	9,58
Inpp5d	SHIP-	10,56
lfngr1	lfgr	11,88
Card11	BIMP3	15,03
Ski	2310012I02Rik	21,26
Socs1	SOCS-1	70,52

**Supplementary table 4**(B) Genes downregulated in miR155<sup>-/-</sup> BMDM compared to wildtype BMDM.

<b>Symbol</b>	<b>Gene name</b>	<b>Fold regulation</b>
Fgf7	Kgf	-98,36
Cyr61	CCN1	-15,35
Hnrnpa3	2410013L13Rik	-9,32
Tceb1	2610043E24Rik	-6,36
Zmym2	Zfp198	-6,11
Mlh1	1110035C23Rik	-6,06
Lpar6	2610302I02Rik	-5,94
Tomm20	1810060K07Rik	-5,82
Msh6	Gtmbp	-5,62
Ttl	2410003M22Rik	-5,21
Uqcr11	0710008D09Rik	-4,82
G3bp2	AA409541	-4,17
Det1	2610034H20Rik	-3,48
Tm6sf1	AI428514	-3,48
Rap1b	2810443E11Rik	-3,39
Matr3	1110061A14Rik	-3,32
Skiv2l2	2610528A15Rik	-3,32
Dhx40	PAD	-3,29
Usp14	2610005K12Rik	-2,87
Sep 11	6230410I01Rik	-2,60
Aak1	5530400K14Rik	-2,31
Kras	Kras2	-2,23
Mecp2	1 Mbd5	-1,71

<b>Symbol</b>	<b>Gene Name</b>	<b>Fold regulation</b>
Zfp652	9530033F24Rik	-1,65
Ets1	AI196000	-1,64
Rhoa	Arha2	-1,54
Smad2	Madh2	-1,32
Aicda	Aid	-1,32
Ndfip1	0610010M22Rik	-1,27
Agtr1a	Agtr1	-1,21
Astn2	Astnl	-1,21
Edn1	ET-1	-1,21
Gdf6	BMP13	-1,21
Ldoc1	Gm366	-1,21
Nova1	Nova-1	-1,21
Pld5	B230365F16Rik	-1,21
Sec14l5	-	-1,21
Sox1	BB176347	-1,21
Stxbp5l	LLGL4	-1,21
Tshz3	Tsh3	-1,21
Zic3	Bn	-1,21
Ilf3	NF90	-1,21
Pea15a	Mat1	-1,16
Meis1	C530044H18Rik, Evi8	-1,14
Pam	PHM	-1,14
Mef2a	A430079H05Rik	-1,07
Rreb1	1110037N09Rik	-1,01



# **Supplementary table 5**

Results of PCR array "Mouse angiogenesis": Comparison of wildtype and miR-155 deficient murine ECs.

(A) Genes enriched in miR-155<sup>-/-</sup> ECs compared to wildtype cells.

Symbol	Gene name	Fold regulation
Ang	Rnase5	2,44
Egf	AI790464	2,44
ErbB2	HER2	2,34
Anpep	Cd13	1,86
Cxcl1	Gro1	1,73
Ifng	IFN-g	1,69
Tgfb1	TbetaR-I	1,51
Lect1	Bricd3	1,43
Csf3	G-CSF	1,10

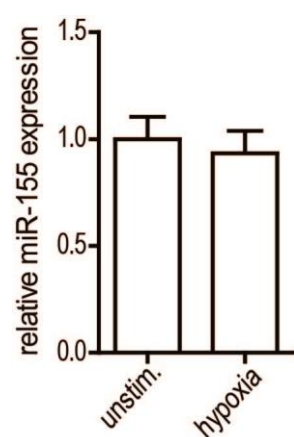
**Supplementary table 5**

(B) Genes downregulated in miR-155 deficient ECs compared to wildtype ones.

<b>Symbol</b>	<b>Gene name</b>	<b>Fold regulation</b>
Mmp9	MMP9	-4,54
Itgb3	CD61	-3,56
Fgfr3	Fgfr-3	-3,16
Tgfa	wa-1	-3,08
Epas1	HIF-2alpha	-3,01
Vegfa	Vegf	-2,97
Fgf1	Fgf-1	-2,95
Nrp1	NP-1	-2,79
Il1b	IL-1beta	-2,79
Angpt2	Ang2	-2,66
Angpt1	Ang-1	-2,66
F2	thrombin	-2,64
Thbs1	Thbs-1	-2,64
S1pr1	Edg1	-2,48
Serpine1	PAI-1	-2,38
Thbs2	Thbs-2	-2,37
Bai1	R75078	-2,33
Fgf6	Fgf-6	-2,33
Lep	ob	-2,33
Plg	AI649309	-2,33
Eng	S-endoglin	-2,28
Fgf2	bFGF	-2,18
Il6	Il-6	-2,16
Jag1	Ser-1	-2,13

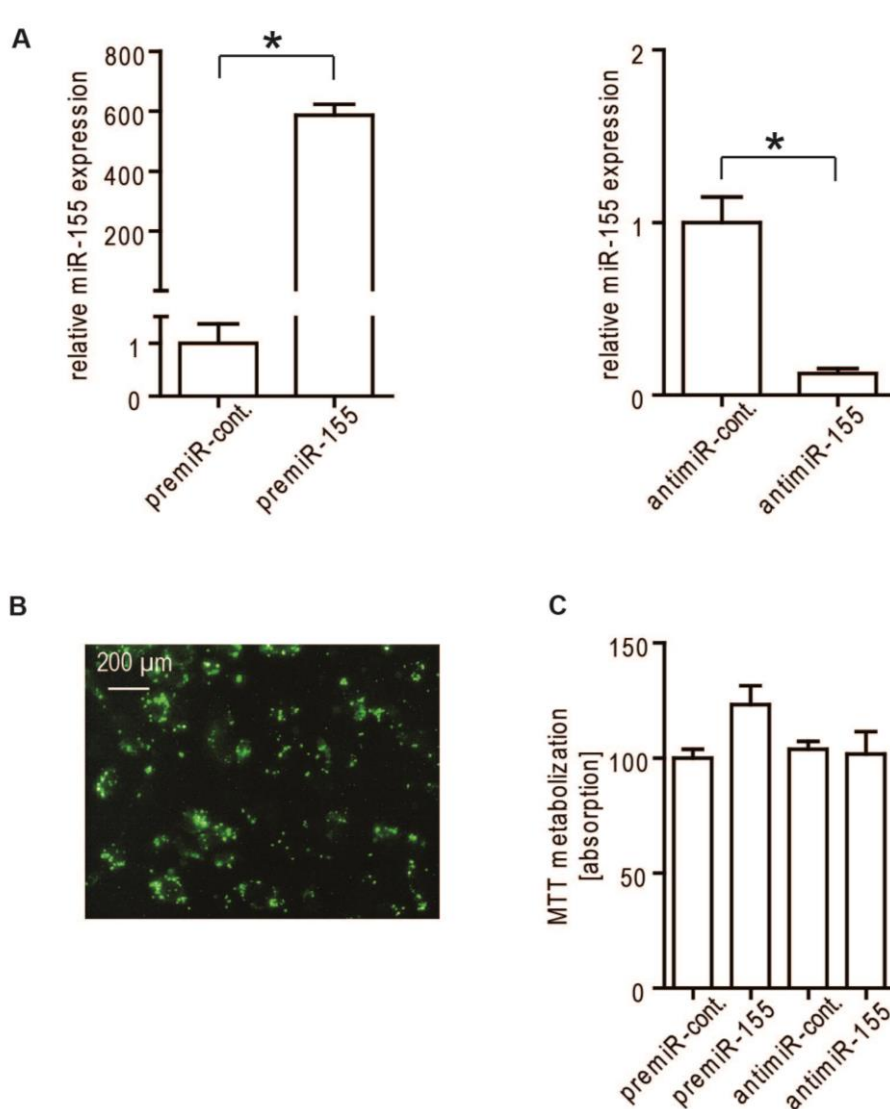
<b>Symbol</b>	<b>Gene name</b>	<b>Fold regulation</b>
Tek	Tie2	-2,09
Smad5	Madh5	-2,02
Mmp2	MMP-2	-2,00
Ephb4	Myk1	-1,96
Figf	VEGF-D	-1,96
Ctgf	Hcs24	-1,93
Nos3	eNOS	-1,86
Vegfc	VEGF-C	-1,84
Flt1	VEGFR-1	-1,83
F3	Cf-3	-1,81
Mapk14	p38-alpha	-1,81
Cdh5	VE-Cad	-1,81
Tgfb1	Tgfb-1	-1,77
Tgfb2	Tgfb-2	-1,76
Tie1	tie-1	-1,74
Cxcl2	MIP-2	-1,66
Ccl11	eotaxin	-1,66
Hgf	HGF	-1,64
Igf1	Igf-1	-1,64
Kdr	VEGFR-2	-1,63
Sphk1	Spk1	-1,59
Serpinf1	Sdf3	-1,56
Hif1a	HIF1alpha	-1,56
Edn1	ET-1	-1,53
Nrp2	Npn2	-1,53
Tgfb3	Tgfb-3	-1,52

<b>Symbol</b>	<b>Gene name</b>	<b>Fold regulation</b>
Itgav	CD51	-1,50
Mdk	MK	-1,48
Vegfb	VEGF-B	-1,46
Pgf	Plgf	-1,46
Col18a1	-	-1,45
Cxcl5	ENA-78	-1,44
Ccl2	MCP1	-1,40
Akt1	Akt	-1,35
Pecam1	PECAM-1	-1,33
Timp1	TIMP-1	-1,32
Col4a3	alpha3(IV)	-1,31
Pdgfa	-	-1,29
Efna1	Efl1	-1,23
Fn1	Fn-1	-1,23
Timp2	Timp-2	-1,22
Tnf	TNF-alpha	-1,20
Ptgs1	COX1	-1,19
Plau	u-PA	-1,15
Tymp	Pdgfec	-1,15
Mmp19	-	-1,11
Efnb2	Lerk5	-1,10
Tnfsf12	Tweak	-1,09
Tbx1	-	-1,07
Mmp14	MT-MMP-1	-1,03
Ptk2	FAK	-1,02



### Supplemental figure 1

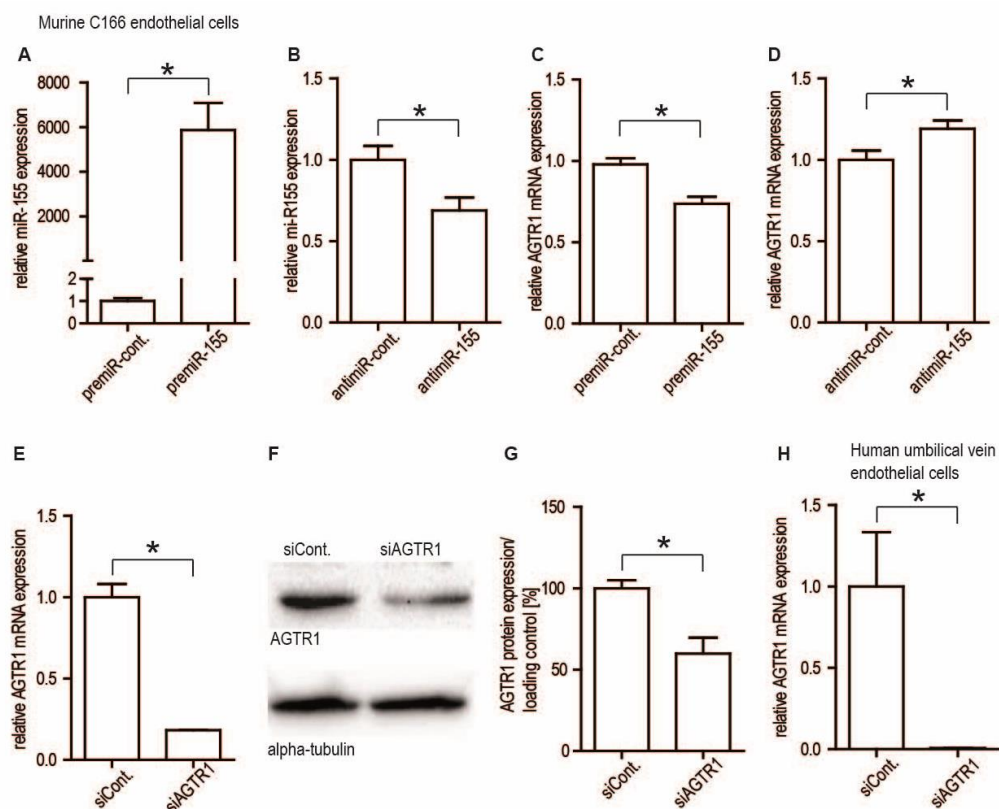
MiR-155 expression under hypoxic conditions in murine ECs was determined by stemloop-based taqman PCR (n=4). Data represent mean values with SEM. \*P<0.05 vs. the corresponding control.



## Supplementary figure 2

MiR-155 transfection efficacy as determined by stemloop-based taqman PCR (A).

Fluorescent-labeled precursor-control oligonucleotide was transfected and green spots indicated successful transfection (B). Cell-viability following transfection of human umbilical vein endothelial cells (C, n=3). Data represent mean values with SEM. \*P<0.05 vs. the corresponding control.

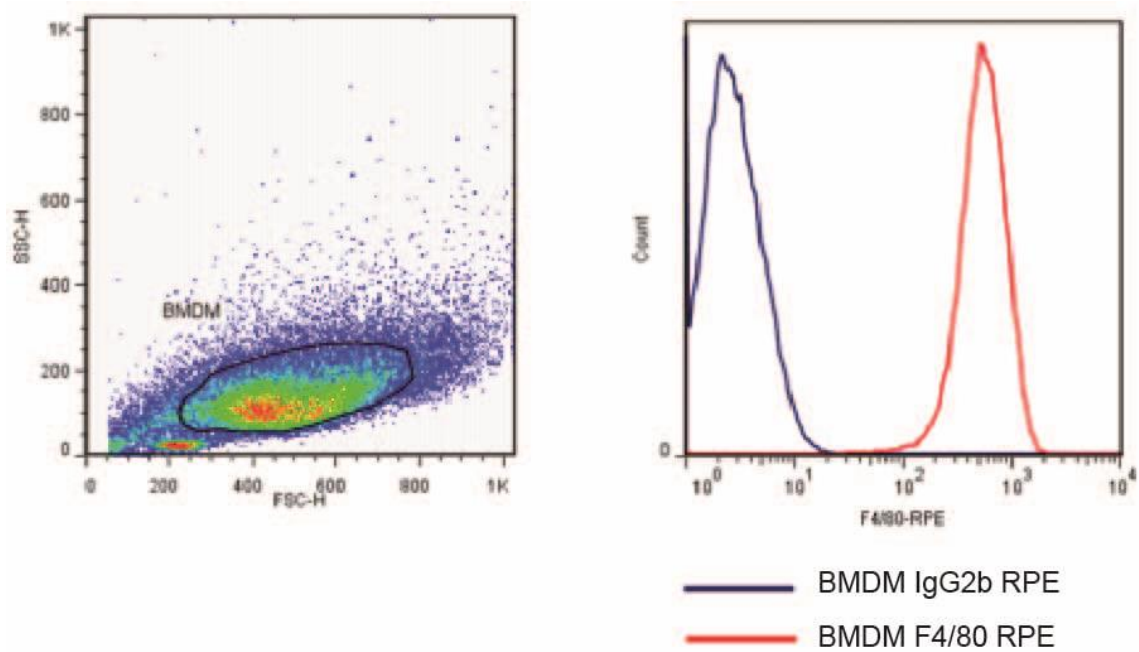


### Supplementary figure 3

MiR-155 transfection efficacy in murine C166 ECs (A+B, n=4). Modulation of miR-155 expression level in C166 murine ECs resulted in expression change of AGTR1 as determined by real-time PCR (C+D, n=4). Silencing efficacy of AGTR1 by siRNA approach in murine ECs on mRNA (E, n=3) and protein level (F+G, n=4) and in human umbilical vein endothelial cells (H, n=3)

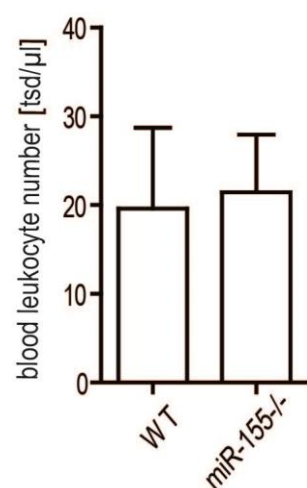
Data represent mean values with SEM. \*P<0.05 vs. the corresponding control.





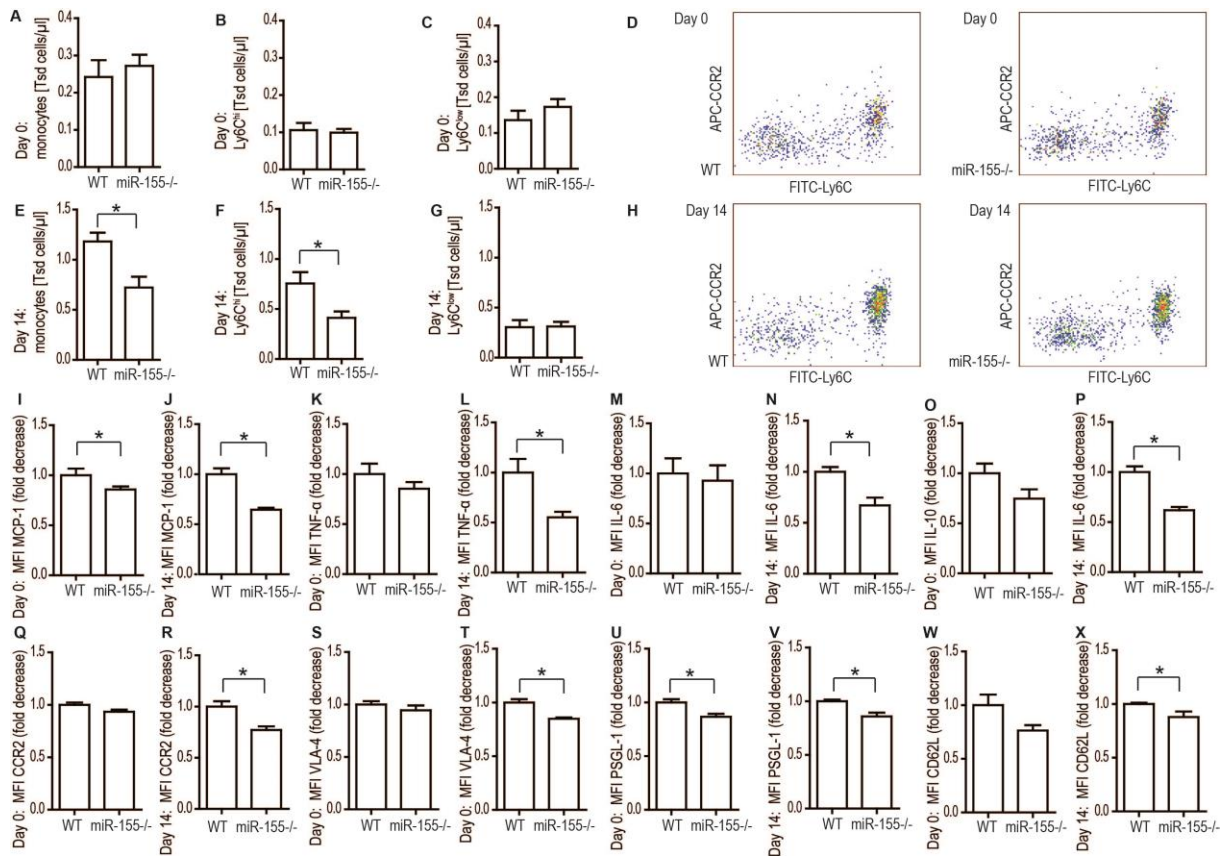
#### Supplementary figure 4

Purity of isolated and cultured murine bone marrow derived macrophages. Bone marrow cells were differentiated to macrophages by stimulation with 30ng/ml of monocyte colony stimulating factor number 1 (MCSF-1) for three days. To confirm the successful differentiation, cells were analyzed for expression of the macrophage marker F4/80 by flow cytometry using RPE-conjugated antibodies against F4/80 and the corresponding negative control IgG2b.



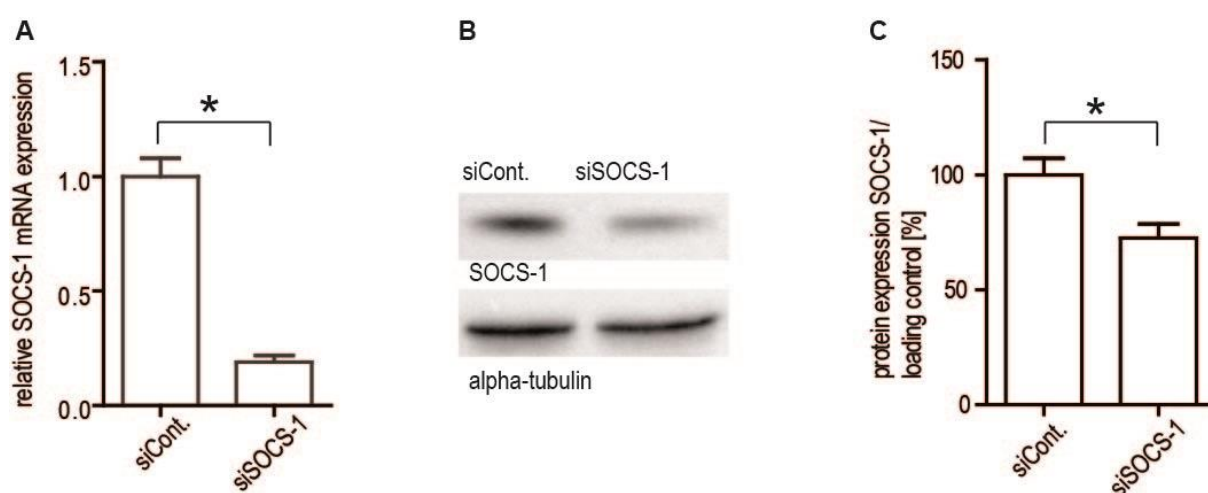
### Supplementary figure 5

No difference in baseline blood leukocyte count was detected in miR-155<sup>-/-</sup> mice compared to wildtype ones (n=6). Data represent mean values with SEM. \*P<0.05 vs. the corresponding control.



### Supplementary figure 6

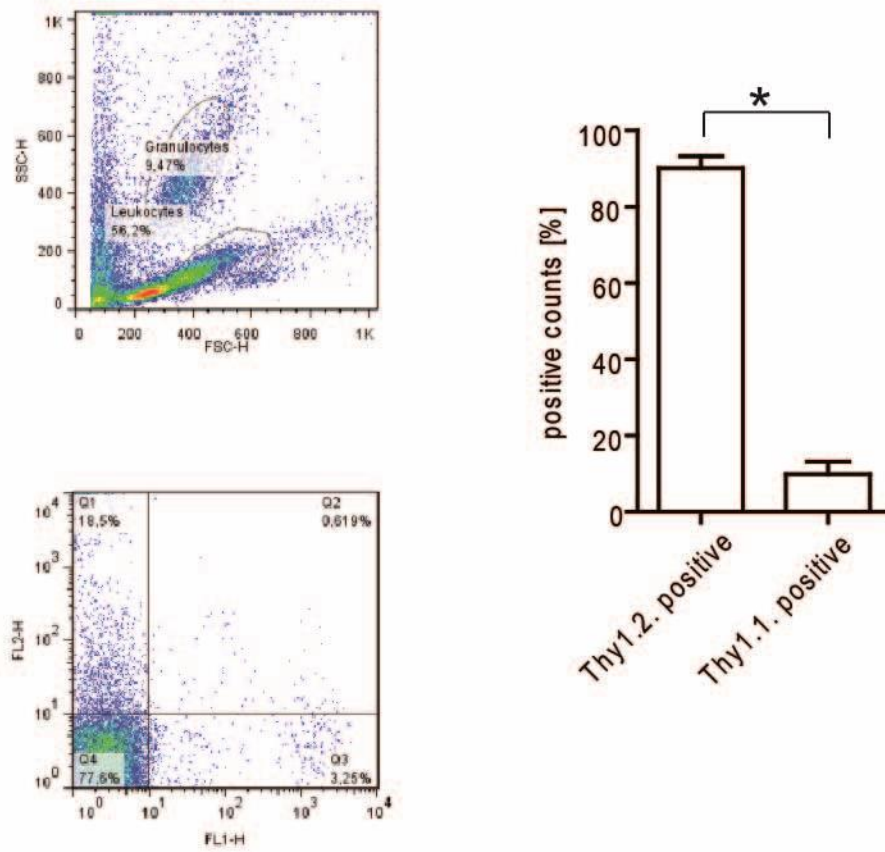
At baseline no difference in total monocyte count as well as in Ly6C<sup>hi</sup> and Ly6C<sup>low</sup> number could be detected (A-C), whereas total number of monocytes as well as Ly6C<sup>hi</sup> subpopulation was significantly reduced at day 14 following femoral artery ligation as determined by flow cytometry (E+F, n=5). Representative examples of Ly6C<sup>hi</sup> and Ly6C<sup>low</sup> monocyte subpopulations in wildtype and miR-155 deficient mice at baseline and at day 14 following hindlimb ischemia (D+H). Measurement of intracellular cytokines/chemokines in Ly6C<sup>hi</sup> monocytes revealed significantly reduced MCP-1, TNF-α, IL-6 as well as IL-10 level in miR-155 deficient mice at day 14 following hindlimb ischemia (I-P, n=5). CCR-2, VLA-4, PSGL-1 and CD62L were significantly reduced in Ly6C<sup>hi</sup> monocytes of mice lacking miR-155 at day 14 following femoral artery ligation as revealed by flow cytometry (Q-X, n=5).



### Supplementary figure 7

SOCS-1 silencing in bone marrow derived macrophages (BMDM) using RNA interference as shown by mRNA expression level (A) and protein expression level (B+C).

A



### Supplementary figure 8

To test the transplant efficacy in transplantation experiments, recipient C57BL/6 luc mice positive for the T-Cell marker Thy1.1 were irradiated and transplanted with bone marrow cells of donor miR-155<sup>-/-</sup> mice positive for the T-Cell marker Thy1.2. Eight weeks after transplantation, circulating leukocytes were analyzed by flow cytometry for the presence of Thy1.1 or Thy1.2 (n=3). Data represent mean values with SEM. \*P<0.05 vs. the corresponding control

## References

1. Thum T, Galuppo P, Wolf C, Fiedler J, Kneitz S, van Laake LW, Doevendans PA, Mummery CL, Borlak J, Haverich A, Gross C, Engelhardt S, Ertl G, Bauersachs J. Micrnas in the human heart: A clue to fetal gene reprogramming in heart failure. *Circulation*. 2007;116:258-267
2. Grundmann S, Schirmer SH, Hekking LH, Post JA, Ionita MG, de Groot D, van Royen N, van den Berg B, Vink H, Moser M, Bode C, de Kleijn D, Pasterkamp G, Piek JJ, Hoefer IE. Endothelial glycocalyx dimensions are reduced in growing collateral arteries and modulate leucocyte adhesion in arteriogenesis. *Journal of cellular and molecular medicine*. 2009;13:3463-3474
3. Bot PT, Grundmann S, Goumans MJ, de Kleijn D, Moll F, de Boer O, van der Wal AC, van Soest A, de Vries JP, van Royen N, Piek JJ, Pasterkamp G, Hoefer IE. Forkhead box protein p1 as a downstream target of transforming growth factor-beta induces collagen synthesis and correlates with a more stable plaque phenotype. *Atherosclerosis*. 2011;218:33-43
4. Heinke J, Wehofsits L, Zhou Q, Zoeller C, Baar KM, Helbing T, Laib A, Augustin H, Bode C, Patterson C, Moser M. Bmper is an endothelial cell regulator and controls bone morphogenetic protein-4-dependent angiogenesis. *Circ Res*. 2008;103:804-812
5. Grundmann S, Hoefer I, Ulusans S, van Royen N, Schirmer SH, Ozaki CK, Bode C, Piek JJ, Buschmann I. Anti-tumor necrosis factor- $\alpha$  therapies attenuate adaptive arteriogenesis in the rabbit. *Am J Physiol Heart Circ Physiol*. 2005;289:H1497-1505